12-15-2014

Neodymium Isotopic Signature of the Deep Western Boundary Current and the Distribution of Neodymium Isotopes and Concentrations Across Line W

Brian Daniel Duggan
University of South Carolina - Columbia

Neodymium Isotopic Signature of the Deep Western Boundary Current and the Distribution of Neodymium Isotopes and Concentrations Across Line W

By

Brian Daniel Duggan

Bachelor of Science
University of South Carolina, 2012

Submitted in Partial Fulfillment of the Requirements

For the Degree of Master of Science in

Marine Science

College of Arts and Sciences

University of South Carolina

2014

Accepted by:

Howie Scher, Director of Thesis

Seth John, Reader

Claudia Benitez-Nelson, Reader

David Barbeau, Reader

Lacy Ford, Vice Provost and Dean of Graduate Studies

Acknowledgments

We thank Torben Stichel, Katharina Pahnke, Steven Goldstein, and Alison Hartman for their excellent work in the laboratory to produce the data analyzed in this study. Also, we extend our appreciation to Beth Bair at the CEMS laboratory and Wayne Buckley in Dr. Scher's laboratory at USC.

Abstract

The capacity of the neodymium (Nd) $^{143}Nd/^{144}Nd$ ratio to trace modern ocean circulation accurately allows for the assumption that the ratio can also accurately trace paleo ocean circulation. Therefore, a complete understanding of Nd cycling and its effect on the isotopic composition in the oceans is vital. Traditionally, Nd isotopic composition (Nd IC) is considered a conservative property in the open ocean, while coastal and margin environments tend to be dictated by nonconservative exchange processes. However, Nd concentrations ([Nd]) in the open ocean typically display a nutrient like profile, increasing with depth. Such a discrepancy between Nd IC and [Nd] has been referred to as the 'Nd-Paradox'. In this study, Nd IC and [Nd] profiles are presented along the oceanographic section known as Line W, observing the interaction between the poleward flowing Gulf Stream (GS) and the equatorward Deep Western Boundary Current (DWBC) in accordance with the international GEOTRACES program.

Surface Nd IC along the transect suggest mixing between three end members passing through the study area; fluvial (Nd IC ~ -11.03) from the margin, GS (Nd IC ~ 9.1) from the Gulf of Mexico and Caribbean, and subtropical mode water (STMW) (Nd IC ~ -9.5) in the open ocean. Just below the Surface mixed layer a prominent STMW signature, flows from the east through to the subsurface GS. Deeper along the margin, the extremely nonradiogenic Upper Labrador Seawater component to the DWBC remains

Relatively unchanged as it flows equatorward with a predominant -14.87 Nd IC. Classic Labrador Seawater also suggests a relatively unaltered Nd IC, reporting -13.5. However, two over flow water masses, Denmark Strait overflow water and Iceland Scotland overflow water do not conform to conservative mixing.

Throughout the study area, [Nd] shows a surface maximum, consistent with lithogenic deposition. Between ~1000 and 2000 m, concentrations remain relatively consistent, coinciding with Nd IC, as a result of increased horizontal advection. Below 2000 m, [Nd] increase while Nd IC remains relatively consistent, indicative of reversible scavenging onto and off of sinking particles. Resuspended sediment in a benthic nepheloid layer produces an inverse relationship between Nd IC and [Nd], likely resulting from lithogenic material with a nonradiogenic Nd IC deposited to the seafloor.

Table of Contents

List of Figures

Chapter 1. Introduction

The Nd IC (Neodymium isotopic composition) refers to the ratio of $^{143}Nd/^{144}Nd$, which is expressed in epsilon notation (ε_{Nd}) calculated using equation 1.

$$\varepsilon Nd = \left(\frac{\left(\frac{143Nd}{144Nd}\right)sample}{\left(\frac{143Nd}{144Nd}\right)CHUR} - 1 \right) * 10^4 \qquad \text{Equation 1. } \varepsilon\text{Nd}$$

Where CHUR (Chondritic Uniform Reservoir, $^{143}Nd/^{144}Nd = 0.512638$) is derived from a model of the isotopic evolution of chondritic meteorites under the assumption that the isotopic composition of the bulk earth resembles that of chondritic meteorites (Jacobsen and Wasserburg, 1980). With respect to Earth's crust, Nd IC expresses a global heterogeneous distribution; ranging from old granitic cratons with ε_{Nd} values as low as of -56 to newly formed mid-ocean ridge basalts ε_{Nd} value of +13 (Jeandel et al., 2007; Lacan et al, 2012). This heterogeneous distribution of Nd IC is a product of the different crustal ages providing distinctive $^{147}Sm/^{143}Nd$ ratios of the crust at the time of formation. Nd is introduced to the oceans by means of lithogenic inputs like aerosols (Grousset et al., 1992) and fluvial partials (Mearns, 1988). Nd concentrations ([Nd]) in the ocean, largely dissolved, are of the order of 10^{-12} g g^{-1} (10 pmol kg^{-1}). However, Lacan and Jeandel, (2005a) suggest boundary exchange as an additional source of Nd, resulting from dissolution of margin sediment Nd accompanying the removal of seawater Nd. Also introduced to the oceans through hydrothermal inputs, Nd has been shown that authigenic Fe-Mn oxide precipitates actively remove Nd in the vicinity of the vents rendering this

source to be negligible and even possibly a sink (Michard et al., 1983; Piepgras and Wasserburg, 1985).

As the predominant source of Nd to the ocean, the continental heterogeneous distribution is imprinted on the ocean (Jeandel et al., 2007). This capacity of the ocean's to mirror the Nd IC of the proximal lithogenic source is suggestive of a 300 – 1000 years residence time, shorter than that of the mean ocean mixing time (Tachikawa et al., 2003; Arsouze et al., 2009). However, with a nutrient like distribution, [Nd] mimic silicate and other nutrients resulting in Pacific Ocean enrichment relative to the Atlantic Ocean. The nutrient like behavior of [Nd] in seawater is suggestive of a 5000-year residence time, greater than the residence time calculated for Nd IC and the mean ocean mixing time (Bertram and Elderfield, 1993, Siddall et al., 2008). Moreover, this Nd enrichment is not sufficient to account for an Nd IC shift from an unradiogenic -15 in the North Atlantic to a radiogenic -4 in the North Pacific (Lacan et al., 2012). This discrepancy has come to be known as the "Nd paradox", documented and summarized in pervious studies (Bertram and Elderfield, 1993; Jeandel et al., 1995, 1998; Lacan and Jeandel, 2001; Goldstein and Hemming, 2003). Boundary/particle exchange processes have been attributed to explain such discrepancies (Siddall et al., 2008).

Nd isotopes have been used as a water mass tracer of modern and paleo ocean circulation for over three decades (Frank, 2002; Goldstein and Hemming, 2003; Jeandel, 1993; Lacan and Jeandel, 2005a; Pahnke et al., 2008; Piepgras and Wasserburg, 1982; Piotrowski et al., 2012; Rutberg et al., 2000), however the processes that alter the Nd IC in seawater are not yet entirely understood. Nd IC behaves as a quasi – conservative water mass tracer for modern and past oceans (Piepgras and Wasserburg, 1983, 1987;

Jeandel, 1993; Jeandel et al 1998; Goldstein and Hemming, 2003; Lacan and Jeandel, 2004). Conversely, boundary/particle exchange processes along continental margins and the seafloor may alter the Nd IC (Piepgras and Wasserburg, 1987), providing Nd IC behave quasi – conservatively rather than a true conservative tracer. As a result of the quasi – conservative nature of Nd IC, it has become a prerogative of the GEOTRACES program to better understand this system. Recent studies have shown boundary exchange processes to contribute to the Nd IC in the equatorial Pacific near Papua New Guinea (Grenier et al., 2013), and by aeolian dust deposition and bottom sediment resuspention in the eastern north Atlantic (Stichel et al., 2014).

This study presents 134 Nd IC and 76 [Nd] measurements made along an oceanographic section known as Line W, running from Woods Hole, Massachusetts to Bermuda (Figure 1.1). Samples were analyzed in accordance with efforts of the GEOTRACES program, to develop a greater understanding of the mechanisms controlling input, distribution, and internal cycling of trace elements and isotopes. The transect lies along the western North Atlantic margin, intersected by the poleward flowing Gulf Stream (GS) and the equatorward flowing Deep Western Boundary Current (DWBC). This study aims to assess the geochemical cycling of Nd IC and [Nd] along this passive margin, the intersection of two strongly advective water masses, and their interaction with a benthic nepheloid layer. Increased resolution and comprehensive evaluation of internal cycling processes governing Nd IC and [Nd] will provide invaluable insight into the dominant processes governing these variables. With an improved understanding of these processes it can be possible to produce models reconstructions of past ocean circulation with greater accuracy (Arsouze et al., 2010,

2009, 2008, 2007; Jones et al., 2008; Rempfer et al., 2012a, 2012b, 2011; Siddall et al., 2008).

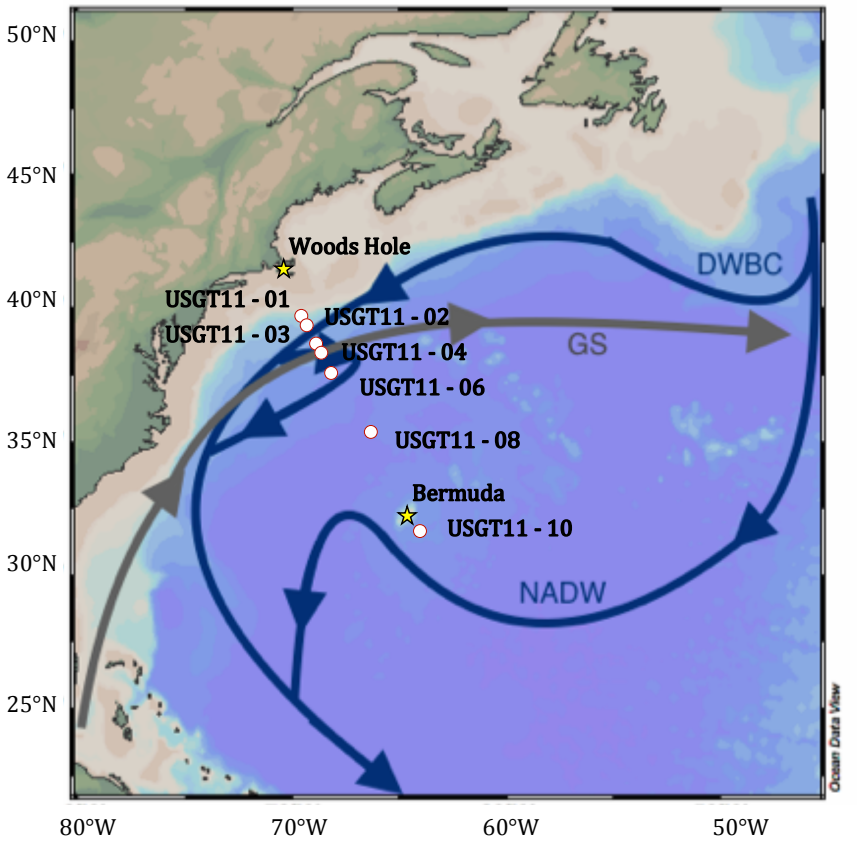

Figure 1.1 Map of the study. The Cruise originating at Woods Hole following along line W, sampling at seven station. Two major components of AMOC, the equatorward DWBC and NADW (blue) passing the poleward GS (grey). The red and white circles signify stations, while the yellow stars indicate Woods Hole and Bermuda. The map was developed using the freely available program *Ocean Data View* (Schlitzer, 2013).

Chapter 2. Hydrography and study area

The study area extends from the North Atlantic western margin by Woods Hole, Massachusetts towards Bermuda and the BATS (Bermuda Atlantic Time Series) station (Figure 1.1). Within this area, two key constituents of the Atlantic Meridional Overturning Circulation (AMOC) are in close proximity to one another, the poleward flowing GS to the east of the equatorward flowing DWCB. From the Straits of Florida, warm waters of the Gulf Stream are transported poleward, separating from the North American margin at Cape Hatteras, North Carolina. Bounded by the Gulf Stream to the east and the North America margin to the west, cool high latitude waters are transported equatorward within the DWBC. The hydrography of the study area has been studied in several previous studies (Stommel, 1965; Schmitz and McCartney, 1993; Pickart and Smethie, 1993; Hwang et al,. 2009; Toole et al., 2011; Peña-Molino et al., 2011) and is only summarized here.

The DWBC located between the GS and the margin, is primarily composed of four water masses: Upper Labrador Seawater (ULSW), Classical Labrador Seawater (CLSW), Iceland Scotland Overflow Water (ISOW), and Denmark Straight Overflow Water (DSOW) (Smethie et al., 2000; Stramma et al., 2004; Lacan and Jeandel, 2005a&b; Joyce et al., 2005; LeBel et al., 2008; Peña-Molino et al., 2011; Van Sebille et al., 2011; Jenkins et al., 2014). ISOW and DSOW have also been defined as North East Atlantic

Deep Water and North West Atlantic Bottom Water, respectively, as other northern water masses composes a portion of these deep waters as they leave the Labrador basin (Lacan and Jeandel, 2005b). However, within this study they will be referred to as ISOW and DSOW with the understanding that these are not pure water masses.

Originating in the Arctic Ocean and Nordic Sea, DSOW and ISOW meet in the Imringer Basin (Tanhua et al., 2005); DSOW sinks beneath ISOW due to its greater density (Table 2.1). These waters meet the Deep Eastern Boundary Current, flowing poleward with an Antarctic Bottom Water constituent, forming the Deep Northern Boundary Current (Lacan and Jeandel, 2005b). The Deep Northern Boundary Current continues into the Labrador basin to meet the final DWBC constituents, CLSW and ULSW. CLSW forms within the Labrador basin through North Atlantic Oscillation induced convection, releasing heat to the atmosphere and sinking as a homogenized mass to ~2000 m (Dickson et al., 1996; Pérez et al., 2008). Further south within the Labrador basin, Pickart et al., (1996) suggest ULSW forms in small eddies near the southwest margin of the Labrador Sea.

In the now fully formed DWBC, each water mass is expressed by a specific Nd IC, [Nd], temperature, and salinity within a defined potential density isopycnal range (table 2.2, Fogelqvist et al., 2003; Lacan and Jeandel, 2005b; Tanhua et al., 2005; Vazquez-Rodriguez et al., 2012). ULSW resides between 400 – 1000 m within the 27.67 and 27.76 kg m^{-3} isopycnals, and is characterized by an ε_{Nd} = -15.00 ± 0.4, [Nd] = 21.5 pmol kg^{-1}, temperature (θ) = 3.5 °C, and salinity (s) = 34.80 psu (practical salinity unit). CLSW is found around 1600 m between 27.76 and 27.81 kg m^{-3} isopycnals and is identifiable by an ε_{Nd} = -13.5 ± 0.4, [Nd] = 17.33 pmol kg^{-1}, θ = 2.95 °C, and s = 34.86

psu. Below the Labrador Sea waters, ISOW flows above DSOW, approximately 2500 m and 3500 m, respectively. ISOW flows within the 27.81 and 27.88 kg m^{-3} isopycnal and is characterized by an ε_{Nd} = -13.2 ± 0.4, [Nd] = 18.03 pmol kg^{-1}, θ = 2.55 °C, and s = 34.97 psu, while DSOW resides below the 27.88 kg m^{-3} isopycnal and is characterized by an ε_{Nd} = -14.5 ± 0.4, [Nd] = 18.03 pmol kg^{-1}, θ = 1.29 °C, s = 34.87 psu. These four water masses then leave the Labrador basin and split; one portion becomes the DWBC continuing south along the margin, while the other continues into the Northern Atlantic to form North Atlantic Deep Water (NADW) (Figure 1.1). Leaving the Labrador basin, ULSW and CLSW are relatively fresh and cool, though as they continue toward the study area, mixing within isopycnals results in increased salinity and temperature (Pickart et al., 1996). Such an increase has been attributed to the Northern Recirculation Gyre (NRG), residing between the GS and DWBC from roughly 500 m to the bottom (Hogg et al 1986; Gangopadhyay. et al., 1997). Interacting with the NGR, the DWBC results with the aforementioned increased salinity and temperature (Pickart and Smethie, 1993).

The GS, also a western boundary current, transports water poleward through the study area. The GS is a warm, saline, rapidly advected current identifiable by a sharp deepening of isopycnals (USGT11 – 03) caused by the large density gradient between the DWBC and the GS (Figure 2.1). To the east of the GS, Subtropical Mode Water (STMW) composes a large water masses within the upper 1000m, also know as '18-degree-water' (Worthington, 1959). To the west of the GS and DWBC, lower salinity water flows off the continental shelf providing an even greater contrast between the GS and water to the west. A few other water masses intersect the study area have been suggested using an optimum multi parameter analysis (OMPA) developed in Jenkins et al., (2014). The

OMPA model suggests small input from Mediterranean Outflow Water (MOW) and Upper Circumpolar Deep Water (UCPDW) throughout the study area. Antarctic Intermediate water (AAIW) and Antarctic Bottom Water (AABW) are transported north as part of the AMOC as well, approximately 1000 m and 3000 m, respectively (McCave and Tucholke, 1986; Tsuchiya, 1989; Pahnke et al., 2012).

Table 2.1 Water mass physical and chimical properties

Water Mass	σ_0 kg/m^3	P. θ °C	P. Salinity pss	θ °C	Salinity psu	Oxygen µmol/kg	Si µmol/kg	References
STMW	–	–	–	18.35	36.42	–	–	e
AAIW	–	–	–	4.37	34.40	188.8	30.99	f
AABW	27.857-27.867c	–	–	0.18	34.70	223.6	116.50	f
ULSW	27.67d-27.76a	4.55b	34.97b	3.50	34.80	296.0	8.35	g
CLSW	27.76-27.81a	3.85b	34.95b	2.95	34.86	293.9	9.20	h
ISOW	27.81-27.88a	2.40b	34.92b	2.55	34.97	277.5	11.00	i
DSOW	>27.88a	2.00b	34.91b	1.29	34.87	298.9	7.50	h
MOW	–	–	–	12.65	36.63	198.4	7.46	f
UCDW	–	–	–	4.28	34.66	155.4	31.64	f
ISW	–	–	–	7.11	35.12	272.4	6.70	h
Coastal water	–	–	–	9.26	34.96	–	–	j

(a) Va´zquez-Rodŕıguez et al., 2012; (b) Smithie et al., 2000; (c) Rickli et al., 2014; (d) Lacan and Jeandel, 2005b; (e) Pahnke et al., 2012 BATS 70 - 500 m; (f) WOCE A07 1993 (g)) AE7W Line; (h) Tanhua et al., 2005; (i) Fogelqvist et al., 2003; (j) Ketchum and Corwin, 1964

Table 2.2 Water mass end member Nd IC and [Nd]

Water Mass	Nd IC εNd	[Nd] pmol/kg	References
STMW	10.10	13.58	a (BATS 70 - 500 m)
AAIW	11.52	15.52	b (Angola Basin)
AABW	-9.10	27.00	c
ULSW	15.00	21.50	d (st. 3 400-1000m)
CLSW	13.50	17.33	d (st. 2 1600m)
ISOW	13.20	18.02	d (st. 6, 2499m)
DSOW	14.50	19.41	d (St. 6, 3501m & 2499m)
MOW	10.60	18.00	e (USGT10 - 01)
UCDW	-8.20	13.88	c
ISW	13.78	17.50	d (St. 14/15/16 upper)
Coastal water	11.30	45.57	f

(a) Pahnke et al., 2012, BATS 70 - 500 m; (b) Rickli et al., 2009; (c) Stichel et al., 2012; (d) Lacan and Jeandel 2005; (e) Stichel et al., 2014; (f) Jeandel et al., 2007

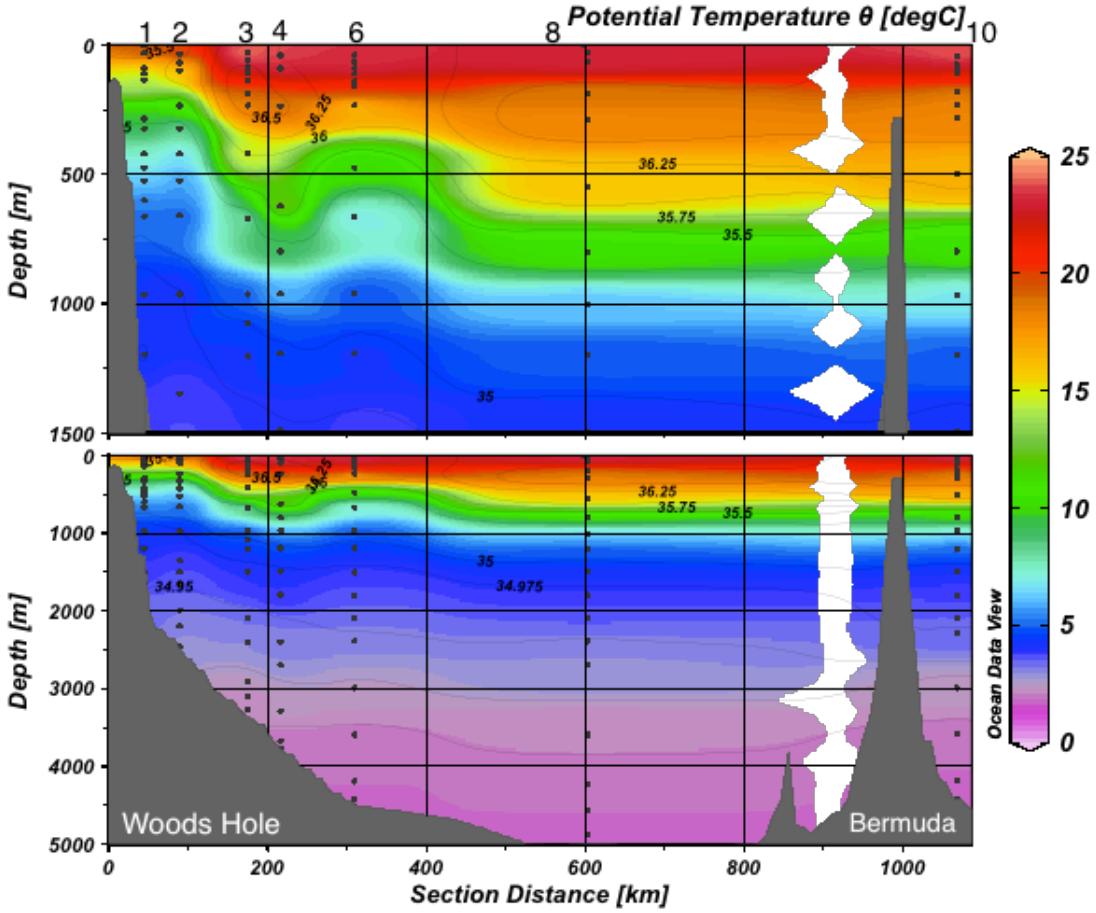

Figure 2.1 Temperature and salinity section. Color shading is representative of potential temperature while contours identify salinity values. Salinity contour line spacing is 0.25 psu between 37 and 35 psu, and 0.025 psu between 35 and 34.9 psu. Station numbers reside over time their perspective site. The plots was developed using the freely available program *Ocean Data View* (Schlitzer, 2013).

Chapter 3. Methods

3.1 Shipboard processing

All samples were collected as part of the GEOTRACES program along the cruse transect of KN204A (November to December 2011), with seven full water column stations (Figure 1.1.). Pahnke et al. (2012) provides a detailed description of the sampling procedure and equipment. 10-L standard General Oceanics Niskin bottles with 0.25mm think nylon coated stainless-steel springs, Viton O-rings at the end caps and spigots mounted on a 24-position powder-coated stainless-steel rosette frame. Dual temperature and conductivity sensors, an SBE43 oxygen sensor, and a Seapoint STM turbidity sensor were used to collect *in situ* data. Seawater samples were filtered through ArcroPak500 (0.8/0.45 μm) filter cartridges into acid-cleaned LDPE containers. Cartridges are initially cleaned with acid and then are reused at each station for a specific depth, only being rinsed with 0.5L of sample before use. Each bottle was used to provide the following aliquots, one ~4L aliquot for thorium and protactinium analysis (Hayes et al., 2014), one ~4L aliquot for Nd isotope and concentrations, and one aliquot to be kept as an archive sample. Using ultra-clean 6N hydrochloric acid, samples were acidified to a pH < 2. Then samples were sealed, double-bagged, and stored for transport to their respective destinations. A procedural blank of 18.2 MΩcm water (Millipore) from Lamont-Doherty Earth Observatory (LDEO) was acidified and stored. The blanks ranged between 30 and

100 pg Nd, lower than the smallest sample size of 8 ng Nd, therefore, no blank correction was applied.

3.2 Analytical methods

Samples where analyzed in three different laboratories: University of Hawaii (UH), Lamont-Doherty Earth Observatory (LDEO), and University of South Carolina (USC), each of which utilizing a slightly different procedure. All three labs sampling techniques are comparable with the successful participation in the GEOTRACES intercalibration during 2008 and 2009 (van de Flierdt et al., 2012). In Pahnke et al. (2012), an intercalibration at the BATS station between LDEO, UH, and the Imperial College London indicates a strong agreement between laboratories. Using the same techniques from the calibrations, we can assume the data is comparable to one another.

UH and LDEO used 20 mg cleaned iron (Fe) in the form of $FeCl_3$ solution and a Nd spike (^{146}Nd at UH and ^{150}Nd at LDEO) with a known weight were added to each sample. Samples were then allowed 2 – 5 days to equilibrate the Fe enrichment and spike, at UH and LDEO, respectively. The pH of each sample was then raised to ~8.5 in order to induce co-precipitation of Nd with FeOOH. The precipitation reaction was allowed to continue between 1 and 5 days at LDEO, after which the supernatant was discarded. Salts were removed from the FeOOH precipitate by means of two Millipore water rinses at a pH of 8. The pH of the Millipore water was adjusted with a purified NH_4OH solution. Following each wash, the solution was centrifuged and the supernatant discarded. 15 ml Teflon vials were used to evaporate the samples to dryness, and then reconstituted in 400 µl aqua regia (UH) or 1 ml 8N HNO_3 (LDEO). In order to break down organic compounds, samples were capped and left on a 110°C hot plate for 24 hours. Samples

were then heated to dryness and reconstitutioned twice with 1ml 6N HCl converting samples to Cl^- (UH only). At UH Fe and other major cations, like barium, are removed through chromatographic separation on a 1.5 AG50W-X8 Biorad bed (200-400 dry mesh). At LDEO, Fe(III) was reduced to Fe(II) with L-ascorbic acid (Arcos Organics). Lastly, Nd was isolated using 250 µl of RE-Spec® resin (100 – 150 µm).

At USC, a ~500 ml aliquot was removed from each sample and stored for analysis of Nd concentrations. Nd and other REEs were extracted from the remaining 4.5 L with C-18 cartridges (Water Inc.) loaded with 300 mg of a REE complexing agent, bis(2-ethylexyl) hydrogen phosphate (HDEHP) (Shabani et al., 1992). 4.5 l of each sample was pumped through the prepared cartridges at a rate of 20 ml/min. Subsequently, the cartridges were washed with 5 ml of 0.01 N HCl to strip barium from the cartridge, the remaining Nd and REEs are then eluted with 35 ml of 6 N HCl.

Nd was purified with 0.2 M alpha-hydroxyisobutic acid (Alpha – HIBA) with an adjusted pH = 4.5 on ~700 µl of AG50W-X8 (200 – 400 µm) resin at UH and LDEO. USC lab used 2 ml Eichrom LN-Spec® resin (50 – 100 µm) was used to separate Nd from the remaining REEs (Pin and Zalduegui, 1997).

3.3 Mass spectrometry

The spiked samples were measured simultaneously for Nd concentrations and isotopic composition with a VG-Sector and VG-Sector54 TIMS at UH and LDEO, respectively. Samples were loaded with 1 µl of 2 N HCl on 1 µl of silica gel as an activator on a rhenium filament to measure Nd as NdO^+ ion. At LDEO, sample were run in 12 block series with a target $^{144}Nd^{16}O^+$ intensity of ~300 mV. A closely monitored input of oxygen to the source was applied to increase the ionization efficiency.

Measurements where done in three stages, each of which JNdi-1 was measured repeatedly were $^{143}Nd/^{144}Nd = 0.512083 \pm 0.000015$ (2σ, n = 31), $^{143}Nd/^{144}Nd = 0.512096 \pm 0.000015$ (2σ, n = 29). and 143Nd/144Nd = 0.512083 ± 0.000016 (2σ, n = 30). At UH, samples were measured at 400 to 600 mV on $^{142}Nd^{16}O^{+}$ 18 blocks with 21 ratios in dynamic mode (3 cycles per ratio). Replicate analysis of spiked and unspiked Nd standard JNdi-1 yielded $^{143}Nd/^{144}Nd = 0.512095 \pm 0.000012$ (2σ, n = 29). At USC, Nd IC was measured on a Thermo Neptune Multi-collector ICPMS. During the sample sequencing a JNdi-1 standard was measured every fourth sample. It was aimed to have the same level of Nd as the lowest sample concentration; typically 20ppb with an aimed intensity of 2.5 V on ^{145}Nd with a resulting external error of $^{143}Nd/^{144}Nd$ was 0.000022 (2σ, n=53). A correction was made at each lab for internal mass fractionation with $^{146}Nd/^{144}Nd = 0.7219$ in an exponential mass fractionation law and their respective biases from the accepted value of $^{143}Nd/^{144}Nd = 0.512115$ for the standard (Tanaka et al., 2000).

At USC, Nd concentration measurements were made, using a novel technique developed as a method to extract REE from marsh water (Antle, 2013). To a previously weighed volume of ~30 mL per sample, a precisely weighed amount of 0.942 ppb ^{145}Nd single element spike was added. Neodymium was preconcentrated by adding 100 µl of cleaned Toyopearl AF Chelate 650 resin to each sample. After 24 hours the resin was washed with 1 – 2 ml of superQ water (18 MΩcm), followed by 1 ml of single distilled 1M HNO_3 to elute and collect Nd from the resin. Once removed from the resin, this aliquot was directly analyzed using the Element 2 ICP-MS. Blank samples were prepared with each extraction and analyzed; the average of the blank counts was then subtracted from each measurement. Blanks on average contributed to 0.8% of the overall counts

reported. Accuracy of the analysis was checked with a KNR195-8-2158 (3000m) SAFe sample that yielded an average concentration of 47.55 pmol/kg ± 3% (n=6).

Chapter 4. Results

The [Nd] of all samples range from 13.14 to 29.50 pmol kg^{-1} (Table 4.1, Figure 4.1). Stations USGT11 - 01, USGT11 - 03, USGT11 - 08, and USGT11 - 10 have full water column profiles for [Nd], however, surface data is not available for station USGT11 - 10. With the exception of USGT11 – 01, minimum [Nd] occurs in the subsurface and increases with depth to maximum [Nd] near the seafloor, similar to observations made at AII 109-1, station 30 (Piepreas and Wasserburg., 1987) and the BATS station (Pahnke et al., 2012). Surface [Nd] measurements (<30 m) were made for stations USGT11 – 01 and 08, 19.31 and 18.46 pmol kg^{-1}, respectively. USGT11 – 03 and 10 exhibit similar near surface [Nd] patterns to USGT11 - 01 and USGT11 – 08 and could be suggested to resemble a similar pattern at the surface. [Nd] concentrations decline from the surface maximum to a minimum between 109 m and 417 m. A declining gradient is apparent between USGT11 – 01 and 03, where subsurface minimum declines from 16.72 pmol kg^{-1} to 13.13 pmol kg^{-1}, respectively. The sub-surface [Nd] minimum remains consistent ~13 - 14 pmol kg^{-1} along Line W extending from USGT11 – 03. Below the sub-surface minimum, [Nd] increases and reaches a mid-depth maximum between 500 to 1200 m; of 19.98 pmol kg^{-1} at USGT11 – 01, 18.54 pmol kg^{-1} at USGT - 03, and 17.17 pmol kg^{-1} at USGT11 - 08. The low [Nd] value at USG11 – 03 (~1077 m) is likely an analytical artifact and will not be considered here. The mid-depth [Nd]

maximum exhibits little variability between ~1200 to 2000 m, declining slightly with increasing depth, with the exception of USGT11 – 08. The [Nd] at USGT11 – 08 does show an overall change between 500 – 1500 m. At all stations below 2000 m, the [Nd] increases linearly with depth, at a rate of 1 pmol kg^{-1} per every 154 – 205 m until ~200 to 1000 m above the seafloor. Just above the seafloor, [Nd] varies greatly within the each profile and in comparison to each other. This variability correlates with the decline in transmissometer voltage. Voltage declines are prominent at USGT11-03 through USGT-08 suggestive of a benthic nepheloid layer.

Nd IC range from a minimum of ε_{Nd} = -14.86 ± 0.36 at USGT11 – 01 to a maximum ε_{Nd} = -8.58 ± 0.21 at USGT11 – 08. Overall, USGT11 – 01 exhibits less radiogenic Nd IC than the other stations, similar to its increased [Nd] with respect to the other stations (Figure 4.1). In the surface and sub-surface, Nd IC becomes more radiogenic with increasing distance from the margin. Below ~400 to 800 m Nd IC becomes less radiogenic reaching a minimum between 500 – 1200 m. At ~1100 m at USGT11-03 the Nd IC becomes more radiogenic (~-11) before returning to nonradiogenic values (~-12). Between 1200 m and 2000 m, Nd IC is relatively uniform, ranging from ε_{Nd} = -13.08 to -14.10 with the exclusion of USGT11 – 03. USGT11 – 03 exhibits a more radiogenic Nd IC than the other stations within the given depth range, however, some of the measurements from USGT11 – 03 are associated with large uncertainties (table 4.1). Nd IC increase to approximately ε_{Nd} = -12.64 below 2000 m and remains relatively constant until ~200 – 1000 m above the seafloor where variability increases. Similar to [Nd], Nd IC increased variability near the sea floor coincided with an increased particle density suggested by a declining transmissometer potential. In

general, it is observed that [Nd] and Nd IC maintains an invers relationship near the seafloor. At USGT11 – 08, this invers relationship is not maintained, nearest the seafloor [Nd] decline while Nd IC becomes less radiogenic. This sample is also marked be anomalously high CFC concentrations suggesting a possible contamination during sampling.

Table 4.1 Measured and CTD data

Station	Depth m	θ °C	Salinity psu	Nd IC εNd	error 2 s. d.	[Nd] pmol/kg	oxygen µmol/kg	Silicate µmol/kg	Transms V	σ kg/m^3	CFC-11 pmol/kg
USGT11 - 01											
Latitude: 39.6927, Longitude: -69.8644; MLD: 64 m; Bottom Depth: 2108 m											
	1.5	19.56	35.05	-11.03	0.24	19.31	225	0.88	4.5	24.918	–
	30.2	19.39	34.98	-11.25	0.22	19.26	226.7	0.88	4.5082	24.911	1.314
	89.2	15.81	36.04	-10.53	0.24	16.77	144.3	5.18	4.5772	26.595	1.222
	109.9	14.40	35.86	-10.66	0.24	16.72	144.8	6.15	4.5818	26.772	1.16
	135.4	13.53	35.73	-10.84	0.27	17.04	151.2	6.84	4.5848	26.863	1.158
	285.9	10.03	35.29	-11.01	0.24	17.16	141.4	12.51	4.5948	27.186	0.695
	324.8	8.99	35.18	-11.23	0.24	16.99	143	14.27	4.5915	27.273	0.608
	419.5	7.69	35.12	-12.12	0.24	17.55	166.5	14.07	4.5943	27.426	0.673
	474.7	6.88	35.09	-12.64	0.22	17.91	184.4	13.68	4.5946	27.512	0.84
	523.9	6.16	35.05	-13.26	0.24	18.51	202.8	13.09	4.5931	27.584	1.026
	599.7	5.35	35.01	-14.02	0.24	19.24	234.4	12.02	4.5995	27.653	1.311
	663.7	4.97	34.98	-14.86	0.36	19.84	243.4	11.34	4.5985	27.673	1.543
	964.0	4.42	34.96	-14.43	0.22	19.19	262	10.85	4.5957	27.720	1.68
	1196.8	4.32	34.98	-13.82	0.24	18.73	256.9	11.53	4.5975	27.750	1.34
	1500.7	3.94	34.95	-13.93	0.24	18.32	264.6	11.92	4.5909	27.771	1.32
	1649.7	3.90	34.95	-13.78	0.24	18.29	264.3	12.12	4.5895	27.776	1.257
	1999.0	3.67	34.95	-13.78	0.24	17.98	266.7	13.19	4.5862	27.798	1.041
	2029.9	3.38	34.94	-13.35	0.24	17.78	267.5	14.66	4.5867	27.821	–
	2044.2	3.36	34.94	-13.47	0.45	17.89	268.2	14.76	4.5862	27.822	–
	2048.4	3.62	34.95	-13.87	0.27	17.97	266.5	13.58	4.5866	27.803	1.007

2058.9	3.35	34.94	-13.37	0.24	17.74	267.2	14.85	4.5842	27.823	–
2068.4	3.35	34.94	-13.33	0.22	17.57	267.5	14.76	4.5839	27.824	–
2077.2	3.35	34.94	-13.33	0.31	17.74	267.2	15.15	4.5813	27.824	–
USGT11 - 02										
Latitude: 39.35, Longitude: -69.54; MLD: 61 m; Bottom Depth: 2493 m										
35.6	20.73	35.42	-10.23	0.18	–	222.4	0.78	4.4758	24.896	1.266
69.6	17.25	36.10	-9.95	0.18	–	149.9	3.8	4.5696	26.304	1.303
99.3	14.90	35.91	-10.37	0.18	–		5.75	4.5774	26.706	1.173
235.2	10.52	35.31	-10.20	0.18	–	126.4	12.68	4.5881	27.109	0.707
323.9	8.04	35.13	-11.62	0.18	–	157.3	14.34	4.5858	27.377	0.671
420.2	6.39	35.06	-13.17	0.18	–	196	13.17	4.5912	27.560	0.957
524.0	5.50	35.04	-13.44	0.18	–	221.6	12.3	4.5932	27.656	1.129
657.8	4.97	35.02	-13.71	0.18	–	238.5	11.51	4.5944	27.704	1.227
962.8	4.23	34.97	-13.81	0.18	–	257.9	11.03	4.594	27.750	1.402
1347.8	3.87	34.96	-13.71	0.18	–	262.9	12.1	4.5922	27.782	1.123
1497.3	3.72	34.96	-13.52	0.18	–	264.4	12.78	4.5926	27.795	0.991
1645.9	3.58	34.95	-13.44	0.18	–	265.5	13.17	4.5928	27.804	0.941
1993.4	3.34	34.95	-13.08	0.18	–	265.9	15.42	4.5923	27.830	0.683
2196.3	3.17	34.94	-12.67	0.18	–	266.2	16.69	4.5921	27.843	0.644
2452.2	2.94	34.93	-12.77	0.18	–	269	17.08	4.5807	27.855	0.769
USGT11 - 03										
Latitude: 38.6741, Longitude: -69.1102; MLD: 67 m; Bottom Depth: 3316m										
28.4	24.51	36.17	-9.10	0.34	15.98	204.4	0.68	4.5342	24.375	1.102
61.2	24.15	36.34	-9.52	0.15	15.34	202.8	0.19	4.547	24.616	1.119
86.4	23.59	36.68	-9.55	0.17	15.82	165.7	0.68	4.5692	25.045	1.159
108.8	21.66	36.75	-10.01	0.11	15.26	151.1	1.07	4.5776	25.653	1.218

135.6	20.29	36.76	-10.20	0.30	14.76	161.6	0.78	4.5847	26.040	1.299
186.5	18.95	36.64	-9.91	0.26	14.42	187.8	0.29	4.5875	26.304	1.357
234.7	18.22	36.56	-10.13	0.19	13.14	193.3	0.68	4.5885	26.430	1.391
417.8	15.14	36.02	-11.05	0.25	13.14	170.1	3.51	4.5909	26.751	1.305
668.5	7.52	35.11	-12.55	0.29	17.33	171.1	13.27	4.5925	27.446	0.762
962.8	4.79	35.00	-13.50	0.93	18.54	245.2	11.71	4.5909	27.714	1.343
1077.1	4.52	34.99	-10.99	1.01	16.02	250.5	11.51	4.5932	27.736	1.354
1201.0	4.28	34.98	-10.84	0.26	18.17	258.5	11.42	4.5907	27.751	1.384
1500.0	3.95	34.97	-12.27	1.54	18.13	261.7	12.2	4.5903	27.779	1.119
2096.9	3.40	34.95	-12.76	0.14	17.45	266.9	14.74	4.5895	27.823	0.79
2402.1	3.11	34.94	-12.67	0.68	15.56	266.1	17.47	4.5903	27.850	0.6
2898.2	2.62	34.92	-12.56	0.22	17.97	270.5	19.71	4.5885	27.877	0.749
3109.2	2.41	34.91	-13.22	0.25	21.60	272.2	20.79	4.586	27.888	0.865
3265.3	2.22	34.89	-13.08	0.31	19.56	272.7	20.3	4.522	27.895	0.813

USGT11 - 04

Latitude: 38.3294, Longitude: -68.8607; MLD: 91 m; Bottom Depth: 3789m

39.4	23.54	36.13	-9.70	0.23	−	208	0.39	4.53	24.637	1.128
90.8	23.57	36.14	-9.70	0.48	−	207.8	0.29	4.5271	24.639	1.125
236.7	18.80	36.62	-9.75	0.24	14.49	193.1	0.58	4.5842	26.326	1.344
621.7	13.22	35.72	-10.88	0.27	17.52	161	6.14	4.5896	26.928	1.138
797.4	9.24	35.22	-10.89	0.24	20.93	144.9	13.37	4.5898	27.268	0.656
960.5	6.22	35.07	-13.10	0.26	−	204	12.98	4.5907	27.592	0.938
1191.7	4.74	34.99	-14.00	0.23	−	247.6	11.71	4.5873	27.711	1.462
1488.5	4.28	34.97	-13.80	0.23	−	257.5	11.81	4.5865	27.752	1.364

1790.6	3.99	34.97	-14.10	0.23	−	261.4	12.49	4.5856	27.779	1.123
2394.3	3.43	34.94	-13.50	0.23	−	267.5	14.83	4.5849	27.822	0.827
2697.6	3.21	34.94	-13.00	0.23	−	267	17.08	4.5836	27.844	0.658
3290.7	2.77	34.92	-12.50	0.23	−	270.3	18.83	4.5838	27.873	0.774
3672.3	2.18	34.89	-13.00	0.32	−	266.6	31.52	3.6882	27.897	0.609
3770.6	2.17	34.88	-12.80	0.23	−	264.3	33.86	3.1026	27.897	0.533

USGT11 - 06

Latitude: 37.5874, Longitude: -68.4035; MLD: 109 m; Bottom Depth: 4592m

39.6	23.40	36.00	-9.45	0.18	−	207.7	0.59	4.5241	24.581	1.136
64.6	23.42	36.03	-9.39	0.18	−	207.5	0.59	4.5237	24.603	1.133
89.6	23.46	36.07	-9.61	0.24	−	208.1	0.59	4.5246	24.620	1.128
111.1	23.46	36.08	-9.42	0.18	−	207.4	0.59	4.5319	24.633	1.135
139.6	20.51	36.16	-10.48	0.24	−	175	1.75	4.5738	25.520	1.321
160.0	19.82	36.37	-10.13	0.18	−	166.2	1.95	4.5739	25.867	1.295
232.9	16.07	36.05	-10.49	0.24	−	152.3	4.1	4.5779	26.553	1.288
474.2	10.22	35.30	-10.99	0.24	−	135.9	12.59	4.5846	27.164	0.735
664.2	6.69	35.08	-13.71	0.24	−	191	13.27	4.588	27.533	0.909
960.9	4.91	35.02	-12.77	0.24	−	242.4	11.51	4.5889	27.714	1.321
1191.8	4.39	34.99	-13.75	0.18	−	254.8	11.61	4.5863	27.747	1.338
1503.4	3.93	34.97	-13.49	0.18	−	261.6	12.39	4.5895	27.786	1.08
1797.9	3.65	34.96	-13.28	0.18	−	265.1	13.47	4.5897	27.806	0.913
2092.1	3.44	34.95	-13.14	0.24	−	265.1	15.32	4.5891	27.826	0.726
2385.6	3.19	34.95	-12.82	0.18	−	264.9	17.66	4.5886	27.847	0.546
2989.4	2.69	34.92	-12.35	0.18	−	265.2	21.76	4.5888	27.878	0.459

3590.3	2.31	34.90	-11.95	0.24	–	268.7	26.74	4.5856	27.895	0.53
4191.1	2.21	34.88	-12.58	0.18	–	263.9	34.06	4.5715	27.898	0.424
4423.1	2.21	34.88	-12.77	0.18	–	262.3	36.21	4.5407	27.898	0.392
4517.1	2.21	34.88	-12.83	0.24	–	261.4	37.48	4.3824	27.898	0.379
USGT11 - 08										
Latitude: 35.4159, Longitude: -66.5468; MLD: 98 m; Bottom Depth: 4928m										
1	23.07	36.35	-9.28	0.28	18.46128956	–	–	–	–	–
31.3	23.08	36.35	-8.58	0.21	13.68	210.4	0.39	4.5295	24.943	1.152
68.0	23.07	36.35	-9.25	0.35	14.32	210.4	0.39	4.5327	24.944	1.154
186.3	18.68	36.62	-10.04	0.29	13.48	192.7	0.88	4.5812	26.351	1.355
291.5	18.13	36.59	-9.87	0.45	13.51	209	0.97	4.5816	26.475	1.426
550	15.9854	36.17	-10.31	0.48	17.17	184.4	2.83	–	–	–
800.2	10.43	35.34	-11.26	0.19	16.60	146.9	11.22	4.5873	27.165	0.839
1001.4	6.21	35.06	-13.51	0.18	16.89	201.9	12.88	4.5876	27.590	1.003
1198.8	4.93	35.01	-13.78	0.19	16.38	242.4	11.71	4.5857	27.710	1.335
1495.7	4.32	34.98	-13.38	0.30	17.03	256.6	11.32	4.5842	27.756	1.309
1793.1	3.97	34.97	-13.22	0.21	17.94	262.2	12.2	4.5836	27.784	1.079
2091.9	3.65	34.96	-13.05	0.25	18.14	264.8	13.95	4.5836	27.810	0.844
2391.1	3.29	34.95	-12.83	0.10	16.18	265.6	16.79	4.5828	27.839	0.601
2688.2	3.10	34.95	-12.37	0.24	16.63	263.9	19.42	4.5832	27.857	0.427
3592.3	2.40	34.90	-12.33	0.20	20.88	268.4	25.67	4.5824	27.893	0.405
4232.5	2.27	34.89	-12.43	0.16	24.91	265.4	31.13	4.58	27.899	0.366
4556.1	2.25	34.88	-12.81	0.29	25.63	263.2	34.55	4.5755	27.899	0.336
4880.2	2.22	34.88	-13.72	0.37	21.94	257.5	11.71	4.1924	27.898	1.307
USGT11 - 10										
Latitude: 31.7565, Longitude: -64.1786; MLD: 65 m; Bottom Depth: 4552m										
41.8	24.13	36.55	-9.53	0.22	–	209.1	0.19	4.5343	24.777	1.791
75.7	24.19	36.60	-9.39	0.22	–	209.1	0.1	4.5404	24.807	1.786

89.1	22.12	36.66	-9.64	0.22	–	219.8	0	4.5423	25.458	2.055
109.7	20.55	36.72	-9.98	0.38	13.71	189.7	0.49	4.5568	25.937	2.126
182.4	18.48	36.59	-10.03	0.38	–	203.9	0.49	4.5722	26.383	2.287
233.3	18.25	36.59	-9.80	0.24	–	205.4	0.78	4.5733	26.444	2.276
281.4	18.07	36.58	-10.11	0.24	–	206.4	0.88	4.5739	26.478	2.34
497.1	16.74	36.32	-10.63	0.24	–	193.6	2.05	4.5762	26.616	2.38
796.9	10.53	35.36	-11.32	0.38	17.21	146.8	11.32	4.58	27.160	1.562
969.0	6.77	35.08	-13.03	0.22	18.07	190.1	13.47	4.5812	27.533	1.717
1197.3	5.08	35.03	-13.55	0.22	18.33	238.8	11.81	4.5816	27.707	2.443
1492.8	4.24	34.98	-13.63	0.22	17.77	257.7	12	4.5803	27.765	2.432
1794.0	3.85	34.98	-13.50	0.22	17.08	262.3	13.47	4.5804	27.801	1.816
2094.0	3.61	34.98	-13.03	0.22	16.8	260.4	16.49	4.5802	27.831	1.123
2289.4	3.41	34.97	-12.75	0.38	16.94	260.1	18.93	4.58	27.846	0.792
2990.2	2.63	34.92	-12.81	0.38	20.29	266.6	23.13	4.5788	27.882	0.735
3584.0	2.28	34.90	-12.52	0.22	25.18	266.4	29.18	4.5774	27.896	0.871
4178.9	2.20	34.88	-12.72	0.22	28.73	262.8	35.33	4.5612	27.898	0.757
4419.3	2.21	34.88	-12.65	0.38	28.87	262	36.89	4.5549	27.898	0.681
4431.4	2.21	34.88	-12.84	0.38	–	262.2	36.69	4.5483	27.898	–
4461.6	2.21	34.88	-12.48	0.24	–	262.2	36.4	4.5466	27.898	–
4493.0	2.22	34.88	-12.35	0.24	–	262.1	36.79	4.5461	27.898	–
4511.0	2.22	34.88	-12.76	0.24	29.5	262.2	36.89	4.5455	27.898	–
4522.5	2.22	34.88	-12.58	0.22	28.97	261	37.18	4.5537	27.898	–
4530.9	2.22	34.88	-12.94	0.24	–	261.6	36.99	4.5455	27.898	–
4550.4	2.22	34.88	-12.79	0.24	–	261.6	37.18	4.5453	27.898	–

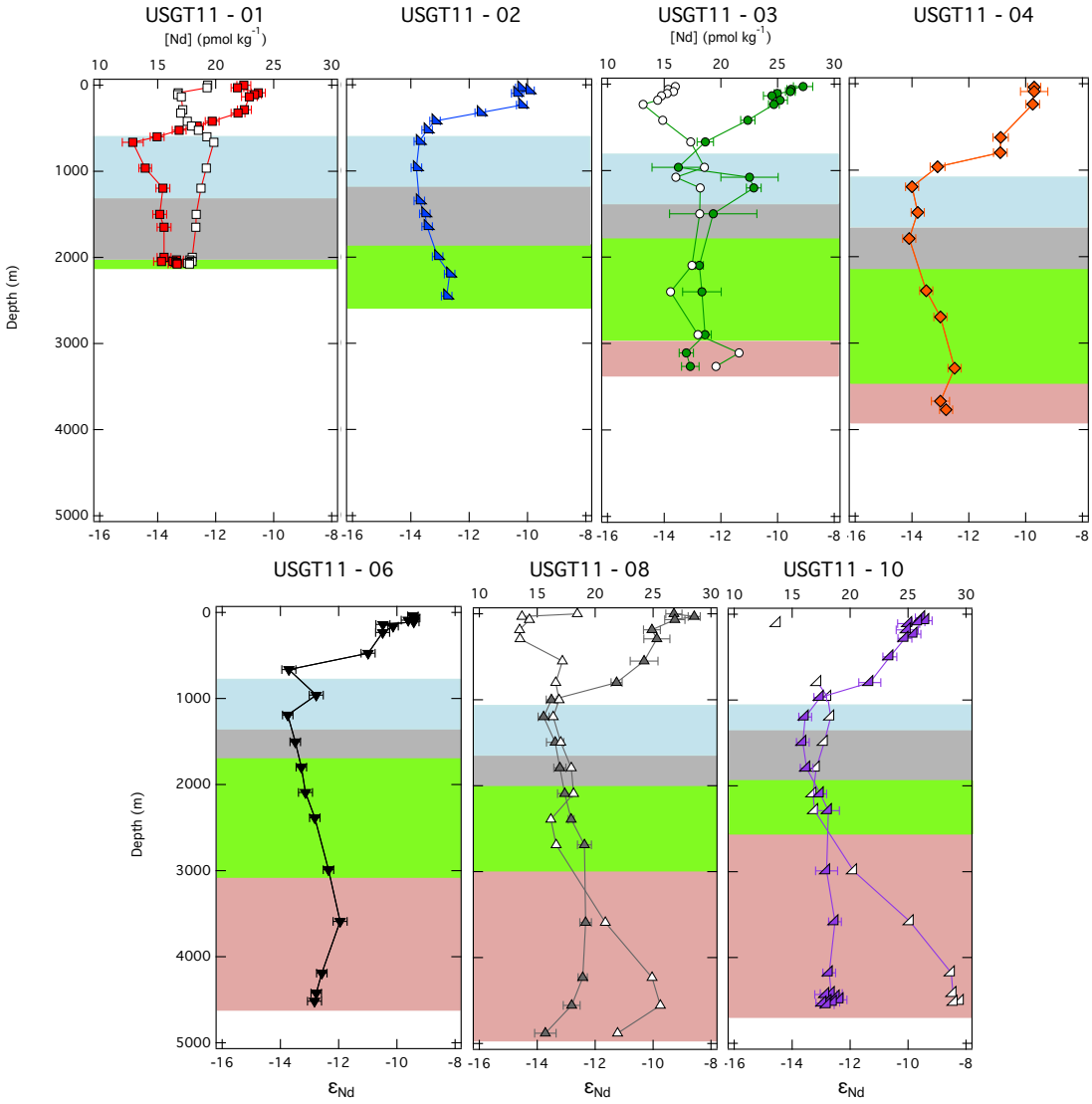

Figure 4.1. Station profiles. Profiles of Nd IC (closed symbols) and [Nd] (open symbols). Color shading refers to the defined potential density range for each of the DWBC water masses. Where blue represents ULSW ($27.67 \leq \sigma_\theta \leq 27.76$), grey represents CLSW ($27.76 < \sigma_\theta \leq 27.81$), green represents ISOW ($27.81 < \sigma_\theta \leq 27.88$), and pink represents DSOW ($\sigma_\theta > 27.88$)

Chapter 5. Discussion

5.1 Mixed Layer and near Surface water Nd IC

Samples collected throughout the surface mixed layer contain the most radiogenic Nd IC within the entire study area, with a maximum at USGT11 – 08 (Figure 5.1a & b, table 4.1). Here the mixed layer is defined by $\Delta\sigma_\theta \leq 0.125$ kg m^{-3} (Table 4.1) (Monterey and Levitus, 1997). Between USGT11 – 01 and USGT11 – 03, average Nd IC within the mixed layer becomes increasingly radiogenic, from ε_{Nd} = -11.14 to -9.39, respectively (Figure 5.1a). Extending east from USGT11 – 03, Nd IC remains relatively consistent, averaging ε_{Nd} = -9.41. Within the mixed layer, [Nd] also indicates a similar horizontal gradient, with a maximum at USGT11 – 01 (19.31 pmol kg^{-1}) to a minimum at USGT11 – 08 (18.46 pmol kg^{-1}) (Figure 5.1b). Just below the surface, ~30 to 60 m, an even more substantial west to east gradient is observed, from 19.26 pmol kg^{-1} at USGT11 - 01 to an average 14.0 pmol kg^{-1} within the MLD range at USGT11 - 08.

The radiogenic Nd IC gradient and declining [Nd] gradient extending out from the western margin corroborates previous mixed layer measurements. The Nd IC for the mixed layer at the western most station (ε_{Nd} = -11.14, USGT11 – 01) is in agreement with Hudson River sediments (ε_{Nd} = -11.3, Jeandel et al., 2007), suggestive of a North American fluvial input from the margin. The Nd IC of the mixed layer from the most distal station (USGT11-10) is in agreement with nearby data from BATS (ε_{Nd} = -9.2 and [Nd] = 14 at 20 m, Pahnke et al., 2012) and from AII-109-1-Station 30 (ε_{Nd} = -9.5 and

[Nd] = 14.42 at 5m, Piepgras and Wasserburg, 1987).

However, a simple two end member mixing between the margin (i.e., USGT11 - 01) and BATS surface water (USGT11 - 10) cannot account for variations in θ -S in surface waters along Line W as most waters are too warm and fresh, likely requiring a third end member (Figure 5.1c). The Gulf Stream represents a volumetrically important contribution of water to the region. Station USGT11 – 03, marking the intersection of the Gulf Stream with the study area, shows the greatest deviation from the mixing line between margin water and BATS surface waters (Figure 5.1c). Thus, waters from the Gulf Stream may provide a third component to the mixing scheme. Mixing between the three end members can account for most of the θ - S and Nd IC variability in the mixed layer, with a few exceptions. The mixed layer composition near USGT11-02 and USGT11-08 (at 30 m) are more radiogenic than would be predicted by T-S mixing alone (Figure 5.1a).

The east-to-west variability persist below the mixed layer, with a prominent salinity maximum to the east of the GS, corroborating with previous studies to suggest the inclusion of STMW (i.e. eighteen degree water, Worthington, 1959; Fratantoni et al., 2013) to the study area (Figure 2.1), while less radiogenic water from the shelf remains confined to the west of the GS. Average Nd IC and [Nd] for STMW at stations near Bermuda (USGT11 – 08 and 10; ε_{Nd} = -9.97 and [Nd] = 13.49 at 100 m to 300 m) corroborate with measurements made at BATS (ε_{Nd} = -10.1 and [Nd] = 13.6, Pahnke et al., 2012). Within the Gulf Stream, Nd IC and [Nd] (USGT11 – 03; ε_{Nd} = -10.02 and [Nd] = 13.78) also corroborates with those reported at BATS and the aforementioned salinity maximum. West of the GS (USGT11 - 01 and 02) and below the MLD, water is

cooler and fresher than its eastern counterpart at equivalent depths (Figure 2.1). The Nd IC and [Nd] for the station nearest the margin (USGT11 – 01; ε_{Nd} = -10.94 and [Nd] = 16.98 pmol kg^{-1}) resembling northeastern North American river sediment (ε_{Nd} = -11.3, Jeandel et al., 2007) and water at a Virginia slope station (ε_{Nd} = -10.8 and [Nd] = 15.94 pmol kg^{-1}, Pahnke et al., 2012), likely flowing from the shelf.

5.2 Deep Nd IC variability

Similar to surface observations, Nd IC is increasingly radiogenic extending from the margin. The Nd IC minimum at the margin (ε_{Nd} = -14.86 and [Nd] = 19.84 pmol kg^{-1} , USGT11 – 01) rapidly degrades to USGT11 – 03 (Figure 4.1 and 5.2). This minimum along the margin could reflect a confined ULSW contribution (ε_{Nd} = - 15.0 and [Nd] = 21.5 pmol kg^{-1}; Lacan and Jeandel, 2005b), or nonconservative addition of a nonradiogenic component from the boundary. However, θ – S calculated ε_{Nd} values do not support the addition of a nonradiogenic signal from the boundary (Hartman et al., in prep). A slight difference in concentrations is likely related to scavenging, which does not necessarily affect the Nd IC (Jeandel et al., 1993). The diminishing ULSW Nd IC signal from the margin corroborates the poleward advection of the GS confining ULSW to the margin (Figure 5.2). Moreover, conservative mixing with water located above and below ULSW is evident through a simple ε_{Nd} – S mixing (Figure 5.3). With the exception of the sample at 1196 m at USGT11 – 01, likely influenced by the GS, samples within the ULSW isopycnals fall on the mixing line between ULSW and CLSW and a 20% STMW with coastal water.

Further supporting conservative mixing, hydrographic properties associated with the Nd IC minimum also demonstrate an ULSW component. The potential density

associated with the Nd IC minimum (σ_θ = 27.67 kg m^{-3}) is in line with ULSW indicated by previous studies (table 2.1, Figure 4.1). Moreover, θ – S measurements (θ = 4.49°C and S = 34.97 psu; USGT11 – 01) also corroborate pervious ULSW measurements proximal to the study area (4.1°C < θ < 5.0°C and 34.96 psu < S < 34.98 psu, Weiss et al., 1985; Fine and Molinari, 1988; Smethie, 1993; Smethie et al., 2000). It is important to note that the proximal measured θ and S values are greater than those corresponding to the true end member (table 2.1). Circulation within the NRG could provide the necessary mechanism to elevate temperature and salinity, as the DWBC and GS interact in the NRG (Pickart and Smethie, 1993). Associated with the ULSW isopycnals, a CFC-11 maximum (CFC-11 = 1.68 pmol kg^{-1}, USGT11 - 01) (Table 4.1, Figure 5.2) is an indication of recently ventilated water (Kieke et al., 2007). Forming in close proximity to the study area, in the southern Labrador basin (Pickart et al., 1996), ULSW is considered the youngest of the DWBC water masses and would be expected to reflect a CFC-11 maximum. Moreover, CFC-11 concentrations corresponding with ULSW isopycnals corroborate with values from previous studies in the area (CFC-11 = 1.4 – 1.6pmol kg^{-1}, Smethie, 2000).

While the nonradiogenic Nd IC of ULSW remains constrained to the margin, a deeper (approximately 1200 to 2000 m) more radiogenic Nd IC (ε_{Nd} = -13.5) persist throughout the entirety of the transect (figure 2.1 and 4.1). This Nd IC is indicative of measurements made in the Labrador basin corresponding to CLSW (ε_{Nd} = -13.5, Lacan and Jeandel, 2005b). Moreover, this Nd IC is tracked across study area by isopycnals associated with CLSW (table 2.1, Figure 5.1)). However, like ULSW, only at the margin

does the Nd IC corroborate with hydrographic properties associated with CLSW. Further indicating the confinement of the DWBC to the margin by the GS (Figure 4.1 and 5.3).

At 3000 m along the continental rise (USGT11 – 03 and 04), a local oxygen and CFC-11 maximum suggest a DSOW component (Figure 5.4 and 5.2). The CFC-11 maximum (USGT11 – 03; CFC-11 = 0.865 pmol kg^{-1} at 3109.2 m) corroborates previous DSOW values (0.75 – 0.5 $pmol.kg^{-1}$, Smethie et al., 2000) at the margin. CFC-11 concentrations coupled with the oxygen maximum, support a DSOW component within the DWBC. However, neither the Nd IC nor [Nd] correspond with previous measurements of DSOW (ε_{Nd} = -14.5 and [Nd] = 18.03, Lacan and Jeandel, 2005b), suggesting DSOW IC has been altered along the margin by nonconservative exchange processes. θ – S calculated ε_{Nd} values also indicate nonconservative alterations to the Nd IC (Hartman et al., in prep), suggesting external inputs to the water column.

Further from the margin, nonradiogenic water occupying stations USGT11 – 04 and 06 (ε_{Nd} = -14.1 and -13.71, respectively) likely characterizes recirculated ULSW resulting from the DWBC intersecting with the GS, south of the study area (Figure 5.2). Pickart and Smethie (1993 and 1997) propose the DWBC intersects the GS, recirculating ULSW poleward as a subsurface Gulf Stream or becomes entrained within a warm/cold core eddies. At USGT11 – 04, the aforementioned Nd IC minimum has a σ_θ (27.77 kg m^{-3}) characteristic of CLSW (table 2.1). However, the Nd IC associated with CLSW (Lacan and Jeandel, 2005b; ε_{Nd} = -13.5) is more radiogenic than the measured value. Therefore, the nonradiogenic Nd IC may support Pickart and Smethie's assertion of GS induced recirculation. In line with the recirculation of ULSW, the Nd IC minimum at USGT11 – 04 is shifted towards the ULSW end member, with respect to ε_{Nd} – S mixing

(Figure 5.3). At station USGT11 – 06, lower θ and S, relative to proximal stations (Figure 2.1); suggests the entrapment of cool, fresh, relatively nonradiogenic water from the margin by warm, saline, more radiogenic GS water, typically identified as a cold core eddy (Bower and Hunt, 1999). It then suggests the hydrographic and isotopic composition of the eddy may result from DWBC and GS mixing, between 650 m and 1200 m depth. A simple θ – S mixing between ULSW and the GS support eddy induced mixing (Figure 5.5). Similarly, ε_{Nd} – S mixing between an ULSW (average ε_{Nd} = -14.37 and S = 34.97 psu, USGT11 – 01) and a relatively pure GS end members (ε_{Nd} = -10.89 and 35.21 psu at 800 m, USGT11 – 04), also supports Pickart and Smethie's eddy assumptions. Deeper samples align nearest the ULSW component, while shallower samples shift toward a greater GS end member (Figure 5.5), accounts for most of the θ – S mixing, with a few exceptions. Samples from USGT11 – 06 deviating from the mixing range, may result from poorly constrained end members due to the complex hydrography of the area.

The persistence of an intermediate to deep nonradiogenic Nd IC (ε_{Nd} = -13.44 and [Nd] = 17.60 pmol kg^{-1}, USGT11 – 06, 08, and 10) east of station USGT11 - 03, is suggestive of a Labrador seawater component (Figure 5.2). With respect to simple ε_{Nd} – S mixing, samples within the Labrador Seawater isopycnals suggest an increased Nd IC (Figure 5.3). Moreover, hydrographic properties (i.e. temperature and salinity, θ = 4.28°C S = 34.99 psu) are no longer consistent with ULSW or CLSW, rather, are indicative of upper North Atlantic Deep Water (UNADW) from the BATS station (θ = 6.41°C to 3.49°C and S = 35.02 psu to 34.96 psu, Pahnke et al., 2012). Additionally, UNADW Nd IC at the BATS station (ε_{Nd} = -13.3 and [Nd] = 17.88 pmol kg^{-1}, Pahnke et

al., 2012) is nearly identical to measured values. MOW has been traced north from the Mediterranean Sea, mixing with a Labrador seawater component to form UNADW (Lacan and Jeandel, 2005b). Mixing between the to end members provides a more saline and radiogenic water mass. Based on the Nd IC and hydrographic values, UNADW penetrates the study area, with an equatorward flow, east of the GS. Moreover, radiogenic waters below 2000 m (ε_{Nd} = -12.76) are consistent with a shift toward a lower North Atlantic Deep Water (LNADW) composition (ε_{Nd} = -12.5, Pahnke et al., 2012; Lacan and Jeandel, 2005b). LNADW is a mixed water mass, produced from DSOW, Labrador Seawaters, Subarctic Mode Water, and AABW (Lacan and Jeandel, 2005b). ε_{Nd} - S mixing supports our assertion of LNADW, where deep samples associated with DSOW and ISOW isopycnals are skewed towards the AABW end member (Figure 5.3). However, below 2000 m Nd IC remains relatively consistent, while [Nd] increases linearly, indicative of nonconservative reversible scavenging (Figure 4.1) (Siddall et al., 2008; Tachikawa et al., 1999). Suggesting sinking particles, obtain a coating with the isotopic composition of the surrounding water; Nd is subsequently released with an Nd IC comparable to the water column resulting in increasing [Nd] with a relatively stable Nd IC (Jeandel et al., 1995).

5.3 Surface [Nd] distribution

Dissolved [Nd] at the surface is largely dictated by terrestrial input, whether through aeolian dust or fluvial sediment plumes (Pal singh 2012; Stichel et al., 2014). A local surface [Nd] maximum ([Nd] = 19.31 to 18.46 pmol kg^{-1}) is suggestive of dissolution from terrestrial material. The elevated surface [Nd], with an Nd IC consistent with North American river runoff, declining from the margin suggests a western source

to the area. However, trace element concentrations (i.e. aluminum (Al)), indicative of aeolian and fluvial inputs (Bruland and Lohan, 2003), denote greater concentration in the eastern position of the transect with a maximum at the GS (Measures et al., 2014). Moreover, dust supply to the area primarily originates from the Sahara or North America, neither of which is directly observed with respect to Nd IC (ε_{Nd} = -13.2 ± 0.5 and -14.1 ± 0.3, respectively, Jeandel et al 1995). Measures, (2014) suggest the Caribbean Sea, in line with the Saharan dust plum, receives a large flux of Saharan dust that results in elevated lithogenic material in the surface ocean. Flowing along the relatively radiogenic North American margin (ε_{Nd} = -9, Goldstein and Jacobsen, 1987), the GS may incorporate the radiogenic signal from the margin, resulting in the observed composition. Moreover, USGT11 – 01 surface maximum is likely dominated by riverine input to the continental shelf, indicative of Hudson River sediments (ε_{Nd} = -11.3 and [Nd] = 45.57pmol kg^{-1}, Jeandel et al., 2007;) and Virginia slope water (ε_{Nd} = -10.8 ± 0.5 and [Nd] =15.94 pmol kg^{-1}, Pahnke et al., 2012).

From the surface maximum, [Nd] rapidly decline to a minimum between 100 to 500 m, and maintains the surface gradient extending from the margin. The degree of change between the surface and the minimum increases from the margin, where [Nd] declines by 2.5 pmol kg^{-1} at the margin to nearly 5 pmol kg^{-1} at USGT11 – 08. Stations USGT11 – 03 and 08 the minimum concentrations ([Nd] = 13.14 and 13.47 pmol kg^{-1}, respectively) corroborate with previous measurements made for STMW ([Nd] = 13.58 pmol kg^{-1}, Pahnke et al., 2012). Nearest the margin, STMW Nd IC (ε_{Nd} = -10.66) is associated with the [Nd] minimum; however, concentration values ([Nd] = 16.72 pmol kg^{-1}) do not. If Nd remains conservative, mixing between the overlaying coastal water

and STMW may resolve the observed discordance. In fact, mixing between the Coastal end member and STMW suggest a ~54% mixture (ε_{Nd} = -10.68 and [Nd]= 16.67 pmol kg^{-1}).

5.4 Deep [Nd] control mechanisms

[Nd] profiles below 1000 m demonstrate strong similarities; remaining relatively consistent to ~2000 m, exhibiting only a slight vertical gradient from 18.73 – 18.17 pmol kg^{-1} at 1200m to 18.14 – 16.80 pmol kg^{-1} at 2000 (Figure 5.6a). Nd IC exhibits a similar homogenous signal with depth, with the exception of USGT11 – 03, likely do to its position in relation to the radiogenic GS (figure 2.1 and 4.1). Between USGT11 - 01 and 10, Nd IC expresses a ε_{Nd} between -13.55 and -13.82 at 1200 m to -13.03 and -13.78 at 2000 m, respectively. A vertically homogenized section of the water column is indicative of a well mixed water mass. As discussed in Stichel et al, (2014), if it is assumed reversible scavenging remains constant within a relatively slow transport, it could be expected that concentrations would suggest a nutrient like profile. However, if a portion of the water column maintains strong horizontal advection, such that vertical reversible scavenging is overcome, the resulting section will be vertically homogenized. Such a processes could explain the relatively invariable [Nd] and Nd IC profiles between 1200 – 2000 m. Meridional transport along the margin (Toole et al, 2011) suggest the greatest transport persist within the CLSW density range, calculated to be 9.2 Sv. This water mass in then bounded by slower waters, 4.9 Sv above and 7.6 Sv below CLSW, thus it is assumed similar velocities are associated with UNADW as well.

Below approximately 2000 to 2500 m [Nd] increase at a fairly constant rate, averaging 1 pmol kg^{-1} per every 154 to 205 m (Figure 5.6a). Such rates continue to

increase until 100 to 1000 m above the seafloor where transmissometer data suggest an increase in suspended particles. However, in contrast to concentration profiles at these stations, Nd IC is relatively constant, averaging ε_{Nd} = -12 to -13 (Figure 5.6c). This decoupling of ε_{Nd} from [Nd] has been observed and interpreted in previous studies (Jeandel et al., 2005; Lacan and Jeandel, 2001; Goldstein and Heming, 2003; Stichel et al., 2014) supporting the previously mentioned "Nd-paradox".

Increasing concentrations with depth could suggest a bottom source providing the necessary mechanism for the vertical [Nd] gradient. Pelagic sediments with an authigenic FeMn precipitate obtain the Nd IC of the water column as it settles to the seafloor and increases in size. These FeMn coatings could provide a source of Nd to the water column above; however, it would be expected to detect the highest [Nd] closest to the seafloor as well as FeMn enrichment, which are not observed. Conversely, [Nd] decreases just before the seafloor, possibly caused by the high particle density of a bottom nepheloid layer inferred from transmissometer (table 2.1).

Another possible explanation for the observed [Nd] increase below ~2500 m are variations in the quantity of water through the study area, as previously discussed. Rapid advection will result in a vertically homogenized water mass with respect to [Nd]. While slow-moving water masses with constant dissolution of Nd from sinking particles (i.e. reversible scavenging) could provide the observed [Nd] increase with depth. Using the meridional stream transport calculated by Toole et al., (2011) with the measured [Nd], the highest transport (9.2 Sv; 1 Sv = 10^6 m^3 s^{-1}) coinciding with the 1200 to 2000m invariable [Nd], while slower transport is indicative of deeper water below 2000 m. The deeper, sluggish water would allow reversible scavenging to persist. A vertical flux of

Nd, indicating the dissolution of sinking particles and the release of Nd with depth could support the observed nutrient like profile below 2000 m. Like [Nd], Si often demonstrates a similar profile suggesting the dissolution from sinking particles. Here Nd and Si, increase at relatively the same rate (Figure 5.6b), supporting reversible scavenging. If the sinking particles contain Nd from aeolian dust or river sediment, the IC would reflect that of the end member, Nd IC ε_{Nd} = -11 to -14 (Goldstein et al, 1984; Goldstein and Jacobsen, 1988; Jeandel et al., 1995). As discussed in the previous section, the particles sink through the water column; a coating will develop with a seawater Nd IC. As the particles continue to sink, Nd is released with an Nd IC similar to the water column resulting in the observed distribution (Jeandel et al., 1995; Siddall et al., 2008; Stichel et al., 2014).

5.5 Benthic nepheloid layer

High-suspended particle density at the seafloor between USGT11 – 03 and 10 signified by reduced transmissometer potential is indicative of a benthic nepheloid layer (BNL) (table 2.1, Figure 5.7). The highest particle density at USGT11 - 04 is likely derived from bottom vortices invoked by GS and DWBC interactions. The smallest particle density within the BNL spans the greatest depth range, from 1000 m above the seafloor at USGT11 – 10 (Ohnemus et al., 2014; Gardner et al., 1983). Throughout the BNL, Nd IC and [Nd] deviate from the preexisting trend above this layer. At USGT11 – 03, [Nd] increases at a rate of 1 pmol kg^{-1} for every 205 m, upon entering the BNL [Nd] increases by 2.6 pmol kg^{-1} while Nd IC shifts towards more nonradiogenic Nd IC. However, unlike observations made of eastern boundary BNL, were a sharp increase in [Nd] is companied by a shift toward more radiogenic Nd IC, here [Nd] increase while

Nd IC shifts towards a more non-radiogenic composition nearing the bottom at USGT11 – 03. A similar invers relationship is observed throughout the western BNL, with the exception of the contaminated bottom sample at USGT11 – 08.

The eastern boundary BNL is representative of reductive sedimentary processes, resulting in the release of Nd from authigenic oxides and a shift toward nonradiogenic Nd IC (Stichel et al., 2014). The western BNL is dominated by turbulent resuspention, resulting in extremely high lithogenic concentrations precluding any reductive processes (Ohnemus et al., 2014). Declining Ti/Al ratio near the seafloor reflect proximal effects (i.e. sedimentary release of Al and in situ scavenging on to particles) and distal effects (i.e. lithogenic signatures associated with deep water masses) (Ohnemus et al., 2014). Such processes could provide an explanation for the variability of [Nd] and Nd IC within the BNL. Where bottom sediment, derived from sinking aeolian dust and fluvial particles, suggest a nonradiogenic bottom end member (Jeandel et al., 1995). Providing increased [Nd] as a result of the resuspended sediment within the BNL, would provided the necessary mechanism to produce the observed invers relationship between Nd IC and [Nd].

5.6 Margin exchange

Even though Nd IC is primarily controlled through physical mixing processes, it is necessary to investigate nonconservative additions from the margin as possible control mechanisms (i.e. boundary exchange). Deviations from the end member are associated with similar changes to salinity and temperature, suggestive of mixing between multiple water masses. Basses on θ – S mixing, variability at the margin is primarily accounted for; where ULSW (USGT11 – 01) is 94.5% ULSW, 4.9% Coastal water, and 1.1%

STMW, CLSW (USGT11 – 01) is 75% CLSW and 25% ISOW, and overflow waters are 62% ISOW, 33% DSOW, and 5% AABW. Using the calculated fractions it would be expected that ULSW properties at the margin to be ε_{Nd} = -14.63, [Nd] = 20.93, θ = 4.91°C, and S = 34.99 psu, CLSW at the margin should be ε_{Nd} = -13.43, [Nd] = 16.88, θ = 3.48°C, and S = 34.94 psu, and the overflow waters should reflect an ε_{Nd} = -13.40, [Nd] = 16.96, θ = 2.15°C, and S = 34.90 psu. Though measured data varies little from the calculated values, slight deviations could be induced by boundary exchange.

To account for the slightly more nonradiogenic composition of the measured values, a nonradiogenic source is necessary (ε_{Nd} < -14.63). However, local lithogenic material is too radiogenic to account for either of the Labrador waters, from the bulk North American crust (ε_{Nd} = -9, Goldstein and Jacobsen, 1987) to aeolian dust at the seafloor (ε_{Nd} = -13.2, Lacan and Jeandel, 2005b). The overflow waters may result from such exchange, moreover, there is a large disparity between the predicted and measured [Nd]. It is inferred that, after mixing increases the Nd IC to ε_{Nd} = -13.40 yielding [Nd] of 18.95 pmol kg^{-1} the overflow waters receive lithogenic input. Transport through this depth totals 7.6 Sv (Toole et al., 2011). The additional input necessary to increase the Nd IC to ε_{Nd} = -13.22 and [Nd] = 21.60 pmol kg^{-1} is estimated using equation (2) from Lacan and Jeandel (2005b):

$$\varepsilon_i \times Nd_i \times \varepsilon_a \times F_a = \varepsilon_f \times (Nd_i \times F_w + F_a) \qquad \text{Equation 2.}$$

where ε_i, ε_f, and ε_a are representative of the overflow waters initial, final, and additional Nd IC, respectively. Nd_i is representative of the initial [Nd], and F_w and F_a are fluxes, water mass transport and additional Nd, respectively. Here ε_i = -13.40, ε_f = -13.22, -13.2 ≤ ε_a ≤ -9, Nd_i = 2.73 ppt (18.65 pmol kg^{-1}), and F_w = 7.6 Sv. Such calculations result in

at least 0.88 g s^{-1} for the bulk North American crust (ε_{Nd} = -9) and 161.31 g s^{-1} result from the most nonradiogenic dust contribution (ε_{Nd} = -13.2). Input associated with the nonradiogenic dust may account for the increased Nd IC and 2.64 pmol kg^{-1} difference between the measured data and mixing calculated values. Resuspended sediment from the underlying BNL could supply the necessary flux to the overflow water mass. However, further analysis of the particulate material would provide the additional information to identify possible external sources.

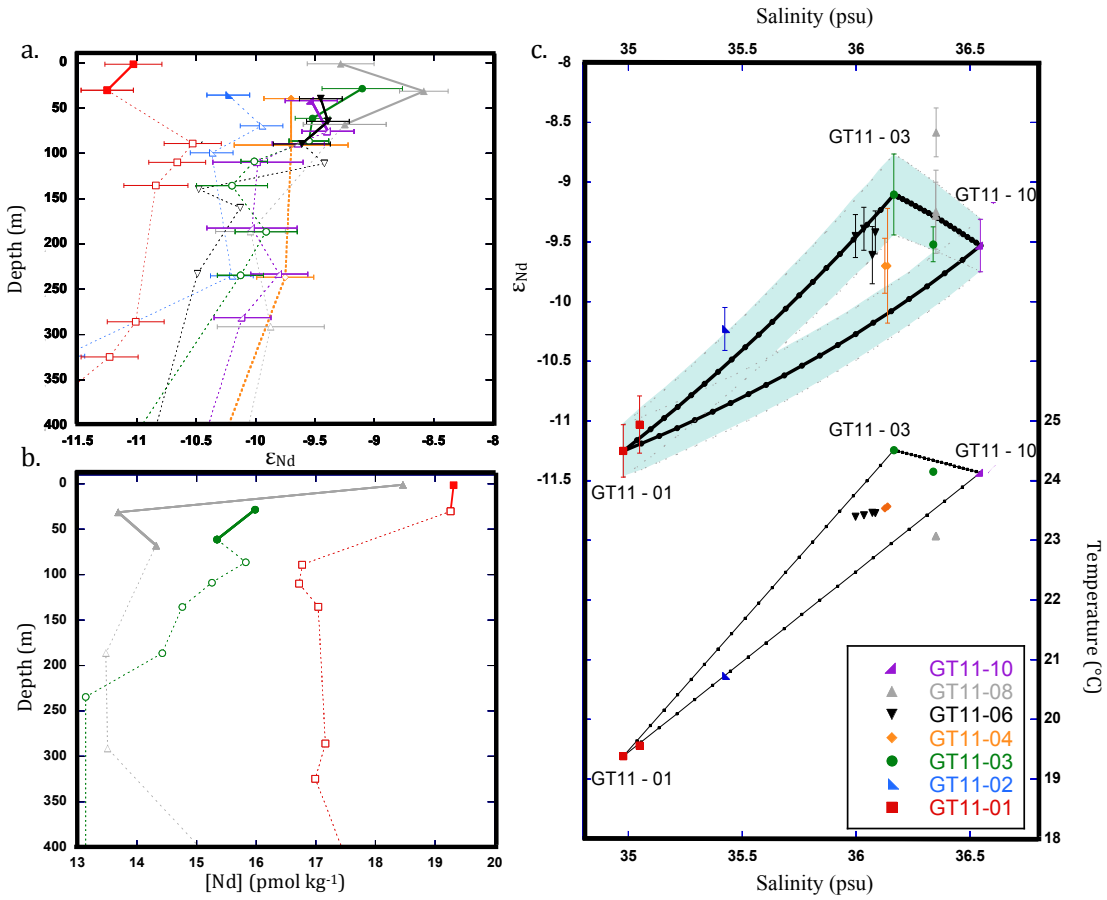

Figure 5.1. MLD Nd profiles and mixing (a) Nd IC is presented as ε_{Nd} values in the top 400 m. (b) [Nd] is presented within the top 400 m. (c. top) ε_{Nd}-S mixing diagram between coastal water (USGT11 – 01), STMW (USGT11 – 10) and the GS (USGT11 – 03). (c. bottom) θ-S mixing diagram between the same end members. Filled symbols are within the mixed layer, while open do not. All symbols corresponded to the legend (c).

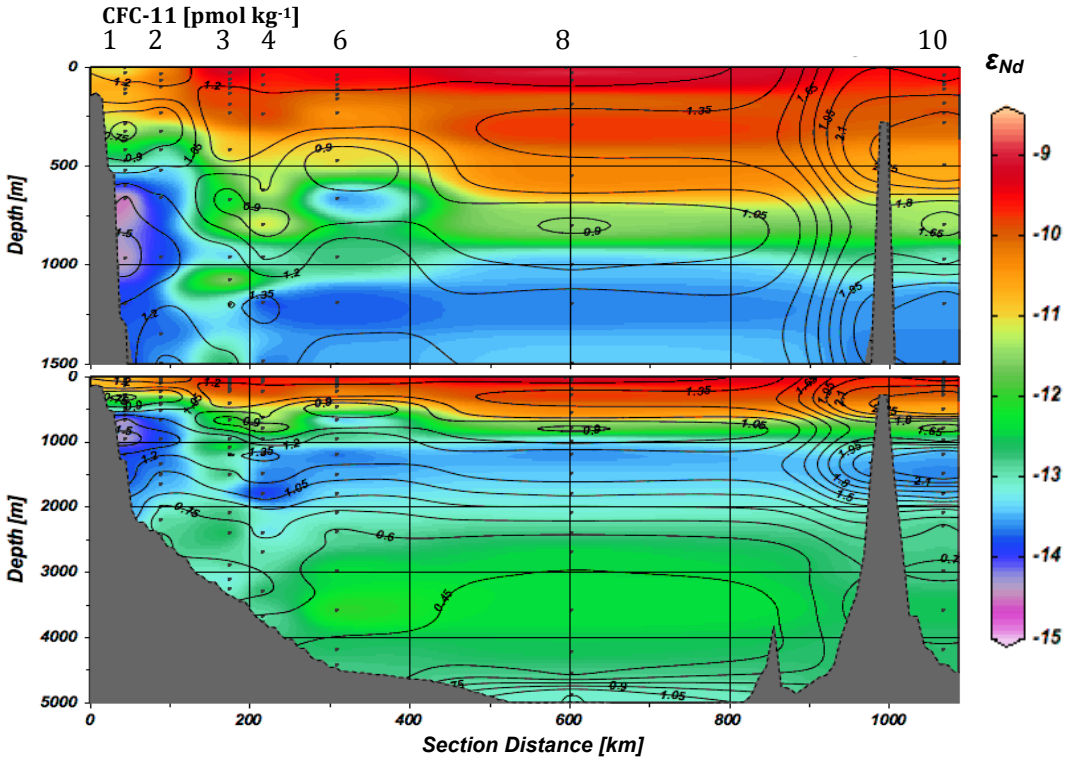

Figure 5.2. Nd IC and CFC-11 (pmol kg^{-1}) section, upper 1500 m on top and the full water column on bottom. Color shading represents ε_{Nd} across the study area overlain are CFC-11 isopycnals. Elevated CFC-11 and ε_{Nd} correspond to the contaminated bottom sample found at USGT11 – 08. The plots were developed with the freely available program *Ocean Data View* (Schlitzer, 2013).

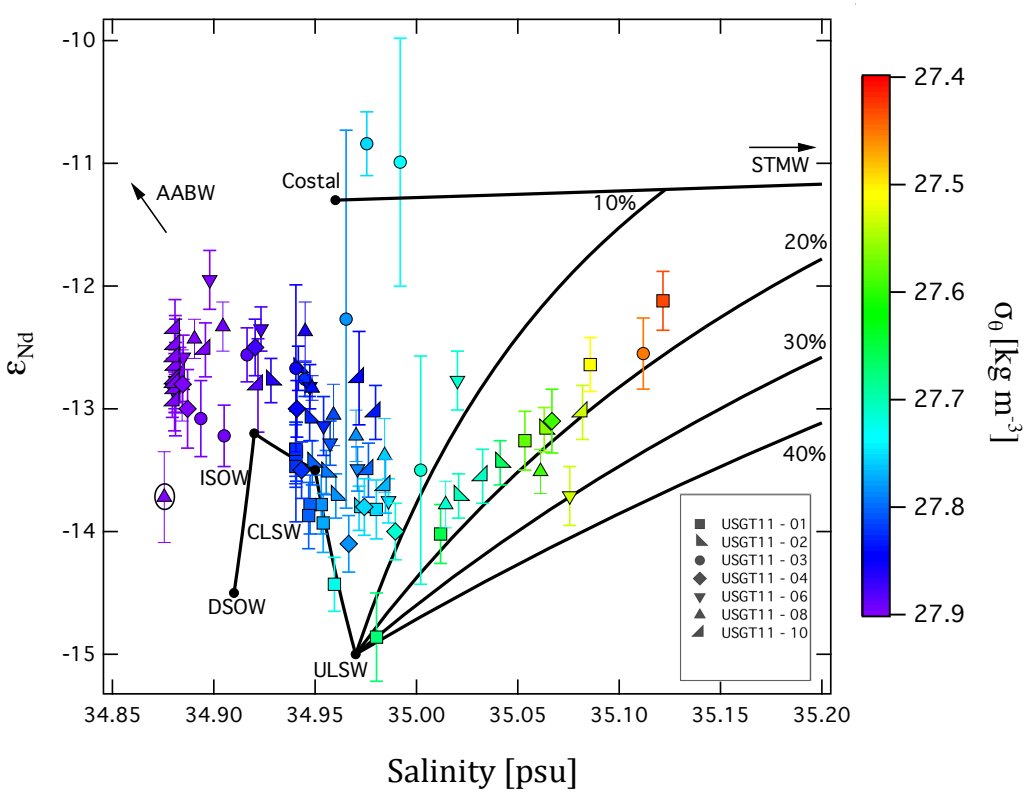

Figure 5.3. ε_{Nd} – salinity, between DSOW, ISOW, AABW, CLSW, ULSW STMW and coastal water (table 2.2). All samples below the thermocline corresponding to $\sigma_\theta \geq 27.40$ kg m^{-3} are shown. Color shading corresponds to σ_θ values. The encircled point from USGT11 – 08 has been suggest to be contaminated and should not be considered.

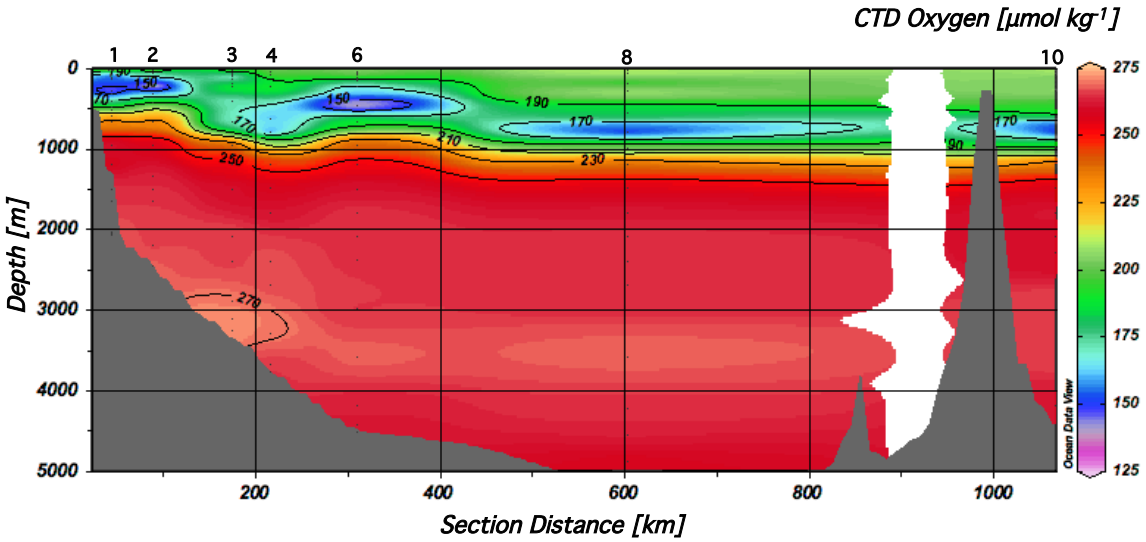

Figure 5.4. Oxygen section. CTD oxygen data across the transect, from Woods Hole (left) to Bermuda (right). Contorts increase every 20 µmol kg^{-1}.

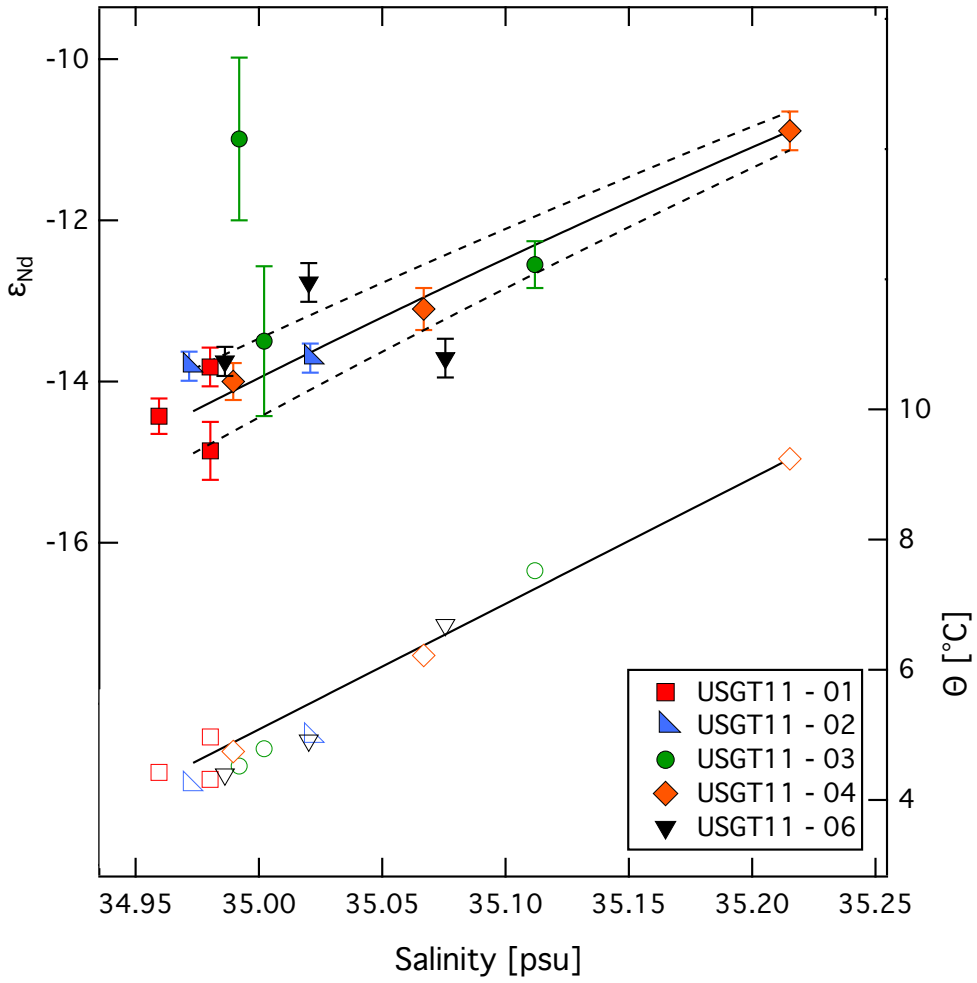

Figure 5.5. ε_{Nd} – Salinity – Temperature mixing. All samples between 650 – 1200 m at USGT11 – 01, 02, 03, 04 and 06 are plotted in this ε_{Nd} – salinity (top) and temperature – salinity (bottom) mixing plot. An average of USGT11 – 01 values provides coastal end member while USGT11 – 04 at 797 m provides the gulf stream end member (table 2.1). Both mixing plots support a mixing between the two end members, excluding the sample at 1088 m at USGT11 – 03.

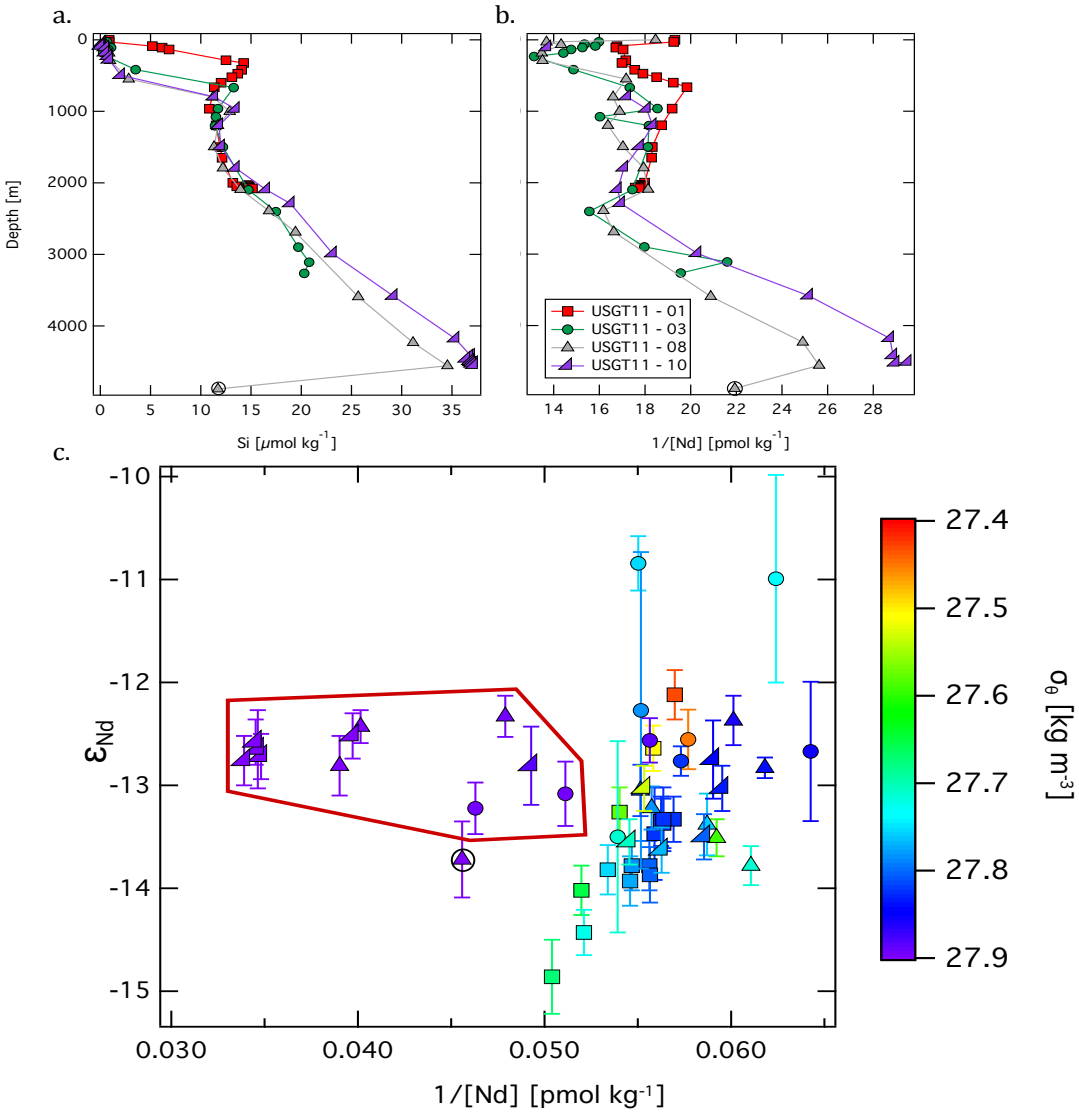

Figure 5.6. Deep [Nd] control. (a) [Nd] (pmol kg^{-1}) profiles (b.) Si (μmol kg^{-1}) (c) All sample within the DWBC isopycnals are plotted within this ε_{Nd} - [Nd] plot. All those located within the red box fall below 3000 m in the water column. Those within the box remain relatively consistent with respect to ε_{Nd}, while [Nd] increase. Samples above 3000 m are in relatively good agreement, with the exception of USGT11 – 03 and 08. The encircled point from USGT11 – 08 has been suggest to be contaminated and should not be considered.

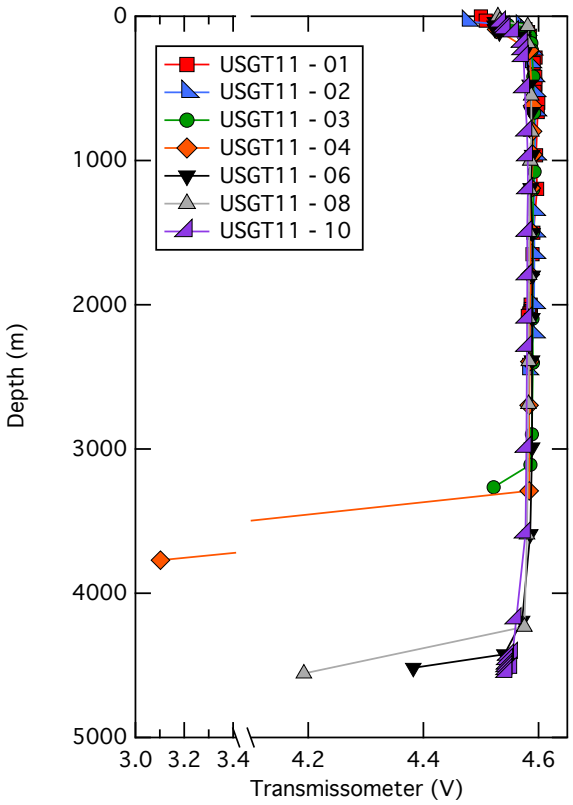

Figure 5.7. Transmissometer profiles. Transmissometer data collected on the CTD providing a proxy for particle density, where decline values suggest an increase in suspended particles.

Chapter 6. Conclusion

This study examines a total of 7 water column profiles for Nd isotopic compositions (Nd IC) and concentrations ([Nd]) along a transect from Woods Hole to the Island of Bermuda, intersecting the equatorward flowing deep western boundary current (DWBC) and the gulf stream (GS). With a vertical sample density >14 samples per station, a high degree of resolution never before seen along the North Atlantic western margin. The findings from these 7 profiles are summarized here.

- Surface values exhibit a horizontal gradient that has been interpreted as a mixing between three end members. Closest to the margin at station USGT11 – 01 a North American shelf signal is prominent, while USGT11 – 10 suggest a STMW end member. A third GS end member intersects the study area at USGT11 – 03 with radiogenic composition, likely derived from the North American curst.
- ULSW flows south along the western margin, expressing the least radiogenic Nd IC within this transect, $\varepsilon_{Nd} = -14.87 \pm 0.36$. Traditional tracers also support the presence of ULSW within the prescribed area. However, ULSW is confined to the margin by the poleward flowing GS. Small fractions of ULSW are then recirculated into cold core eddies or forced down to greater depths by the GS, supporting Pickart and Smethie, (1993) prediction.

- A pronounce CLSW Nd IC throughout the study area, represented be a relatively invariable Nd IC and [Nd]. However, to the east of the GS traditional conservative tracers such as salinity and temperature don't correspond those previously measured. Rather, suggest an upper NADW signal to the east of the GS, and CLSW confined to the margin.
- Within the OW expected isopycnals range, neither Nd IC nor [Nd] support their presence. However, at ~3000 m hydrographic parameters signify a DSOW component to the DWBC, suggesting nonconservative addition to the DSOW water. Within the OW isopycnals Nd IC is relatively invariable depicting a lower NADW signal, while [Nd] increase at a rate of 1 pmol kg^{-1} per every 154 to 205 m. This decupling has been link to reversible scavenging of Nd from sinking particles.
- A benthic nepheloid layer has been observed beneath UST11 – 03, 04, 06, 08, and 10 with a degrading transmissometer potential. An invers relationship between Nd IC and [Nd] within the BNL suggests a removal and addition of Nd from the nonradiogenic resuspended lithogenic particles.

References

Antle R, 2013. Tidal Flux of Transition Metals and Rare Earth Elements from a Barrier Island Salt Marsh. Thesis and Dissertation. Paper 1317.

Arsouze T, Dutay J-C, Kageyama M, Lacan F, Alkama R, Marti O, Jeandel C. 2008. A modeling sensitivity study of the influence of the Atlantic meridional overturning circulation on neodymium isotopic composition at the Last Glacial Maximum. Climate of the Past. p. 191 - 203.

Arsouze T, Dutay J-C, Lacan F, Jeandel C. 2007. Modeling the neodymium isotopic composition with a global ocean circulation model. Chemical Geology. p. 165 - 177.

Arsouze T, Dutay J-C, Lacan F, Jeandel C. 2009. Reconstructing the Nd oceanic cycle using a coupled dynamical – biogeochemical model. Biogeosciences. p. 2829 - 2846.

Arsouze T, Treguier AM, Peronne S, Dutay J-C, Lacan F, Jeandel C. 2010. Modeling the Nd isotopic composition in the North Atlantic basin using an eddy-permitting model. Ocean Science. p. 789 - 797.

Bertram CJ, Elderfield H. 1993 The geochemical balance of the rare earth elements and neodymium isotopes in the oceans 57:1957 - 1986.

Bower SA, Hunt DH. 1999. Lagrangian Observations of the Deep Western Boundary Current in the North Atlantic Ocean. Part II: The Gulf Stream–Deep Western Boundary Current Crossover. Journal of Physical Oceanography. 30. p. 784 – 804.

Bruland KW, Lohan MC. 2003. Controls of Trace Metals in Seawater. Traties on Geochemistry. p. 23 - 47.

Dickson R, Lazier J, Meincke J, Rhines P, Swift J. 1996. Long-term coordinated changes in the convective activity of the North Atlantic 38:241 - 295.

Fine RA, Molinari RL. 1988. A continuous deep western boundary current between Abaco (26.5°N) and Barbados (13°N). *Deep-Sea Res*. p. 1441 – 1450.

Flierdt TVd, Pahnke K, Amakawa H, Andersson P, Basak C, Coles B, Colin C, Crocket K, Frank M, Frank N et al. . 2012. GEOTRACES intercalibration of neodymium isotopes and rare earth element concentrations in seawater and suspended particles. Part 1: reproducibility of results for the international intercomparison. *Limnol. Oceanogr.: Methods*. p. 234 – 251.

Fogelqvist E, Blindheim J, Tanhua T, Østerhus S, Buch E, Rey F. 2003. Greenland–Scotland overflow studied by hydro-chemical multivariate analysis Deep-Sea Research I. p. 73 - 102.

Frank M. 2002. Radiogenic Isotopes: Tracers of past ocean circulation and erosional input. Reviews of Geophysics.

Fratantoni DM, Kwon Y-O, Hodges BA. 2013. Direct observation of subtropical mode water circulation in the western North Atlantic Ocean. 91:35 - 56.

Gangopadhyay A, Robinson AR, Arango HG. 1997. Circulation and Dynamics of the Western North Atlantic. Part I: Multiscale Feature Models. Journal of Atmospheric and Oceanic Teachnology. p. 1314 - 1332.

Gardner WD, Richardson MJ, Hinga KR, Biscaye PE. 1983. Resuspension measured with sediment traps in a high-energy environment. 66:262–278.

Grenier M, Jeandel C, Lacan F, Vance D, Venchiarutti C, Cros A, Cravatte S, 2013. From the subtropics to te central equatorial Pacific Ocean: Neodymium isotopic composition and rare earth element concentration variations. Journal of Geophysical Research: Oceans. 118. p. 592 - 618

Goldstein SJ, Jacobsen SB. 1988. REE in the great-whale river estuary, Northwest Quebec. Elsevier Science. p. 241 - 252.

Goldstein SL, Hemming SR. 2003. Long-lived Isotopic Tracers in Oceanography, Paleoceanography, and Ice-sheet Dynamics Treatise on Geochemistry. p. 453 - 489.

Goldstein SL, O'Nions RK, Hamilton PJ. 1984. A Sm-Nd study of atmospheric dusts and particulates from major river systems Earth and Planetary Science Letters. p. 221 - 236.

Grousset FE, Biscaye PE, Revel M, Petit J-R, Pye K, Joussaume S, Jouzel J. 1992. Antarctic (Dome C) ice-core dust at 18 k.y. B.P.: Isotopic constraints on origins. *Earth and Planetary Science Letters*. p. 203 - 212.

Hayes CT, Anderson RF, Jaccard SL, François R, Fleisher MQ, Soon M, Gersonde R. 2013. A new perspective on boundary scavenging in the North Pacific Ocean. Earth and Planetary Science Letters. p. 86 - 97.

Hogg GN, Pickart SR, Hendry MR, Smethie MW, 1986. The northern recirculation gyre of the Gulf Stream. Deep-Sea Research. 91. p. 7573 – 7585.

Hwang J, Manganini SJ, Montlucon DB, Eglinton TI. 2009. Dynamics of particle export on the Northwest Atlantic margin. Deep-Sea Research I. p. 1792 - 1803.

Jacobsen SB, Wasserburg GJ. 1980. Sm - Nd Isotopic Evolution of Chondrites and Planetary Science Letters. p. 139 - 155.

Jeandel C. 1993. Concentration and isotopic composition of Nd in the South Atlantic Ocean. Earth and Planetary Science Letters. p. 581 - 591.

Jeandel C, Arsouze T, Lacan F, Téchiné P, Dutay J-C. 2007. Isotopic Nd compositions and concentrations of the lithogenic inputs into the ocean: A compilation, with an emphasis on the margins. Chemical Geology. p. 156 - 164.

Jeandel C, Bishop JK, Zindler A. 1995. Exchange of neodymium and its isotopes between seawater and small and large particles in the Sargasso Sea. Geochimica et Cosmochimica Acta. p. 535 - 547.

Jeandel C, Thouron D, Fieux M. 1998. Concentrations and isotopic compositions of neodymium in the eastern Indian Ocean and Indonesian straits. Geochimica et Cosmochimica Acta. p. 2597 - 2607.

Jenkins WJ, Smethie WMJ, Boyle EA, Cutter GA, 2014. Water Mass Analysis for the U.S. GEOTRACES (GA03) North Atlantic Sections. Deep-Sea Research. p. 1–30.

Jones KM, Khatiwala SP, Goldstein SL, Hemming SR, van de Flierdt T. 2008. Modeling the distribution of Nd isotopes in the oceans using an ocean general circulation model. Earth and Planetary Science Letters. p. 610 - 619.

Joyce TM, Dunworth-Baker J, Pickart RS, Torres D, Waterman S. 2005. On the Deep Western Boundary Current south of Cape Cod. Deep-Sea Research II. p. 615 - 625.

Kara AB, Rochford PA, Hurlburt HE. 2000. An optimal definition for the ocean mixed layer depth. Journal of Geophysical Research p. 16803 - 16821.

Ketchum BH, Corwin N. 1964. The persistence of winter water on the continental shelf south of Long Island, New York. Limnology and Oceanography. 4. p. 467-475

Kieke D, Rhein M, Stramma L, Smethie WM, Bullister JL, LeBel DA. 2007. Changes in the pool of Labrador Sea Water in the subpolar North Atlantic. Geophysical Research Letters.

LeBel DA, Smethie W.M, Rhein M, Kieke D, Fine RA, Bullister JL, Min DH, Roether W, Weiss RF, Andrie C, Smythe-Wright D, Jones P, 2008. The formation rate of North Atlantic Deep Water and Eighteen Degree Water calculated from CFC-11 inventories observed during WOCE. Deep-Sea Research. 55. p. 891–910.

Lacan F, Jeandel C. 2001. Tracing Papua New Guinea imprint on the central Equatorial Pacifc Ocean using neodymium isotopic compositions and Rare Earth Element patterns. Earth and Planetary Science Letters. p. 497 - 512.

Lacan F, Jeandel C. 2005a. Neodymium isotopes as a new tool for quantifying exchange fluxes at the continent–ocean interface. Earth and Planetary Science Letters. p. 245 - 257.

Lacan F, Jeandel C. 2005b. Acquisition of the neodymium isotopic composition of the North Atlantic Deep Water. Geochemistry. Geophysics. Geosystems.

McCave N, Tucholke BE. 1986. Deep current-controlled sedimentation in the western North Atlantic. The Geology of North America. p. 451 - 468.

Mearns EW. 1988. A samarium–neodymium isotopic survey of modern river sediments from Northern Britain. Chemical Geology: Isotope Geoscience Section. p. 1 - 13.

Measures C, Hatta M, Fitzsimmons J, Morton P. 2014. Dissolved Al in the zonal N Atlantic section of the US GEOTRACES 2010/2011 cruises and the importance of Hydrothermal inputs. Deep-See Research II.

Michard A, Aldarede F, Michard G, Minster JF, and Charlou JL (1983) Rare-earth elements and unranium in high-temperature solutions from East Pacific Rise hydrothermal vent field (13-degrees-N). Nature. P. 795 – 797.

Monterey G, and Levitus S.1997. Seasonal Variablity of Mixed Layer Depth for the World Oceans. NOAA Atlace NESDIS 14. p. 100.

Ohnemus CD. 2014. Biogeochemistry of Marine Particulate Trace Metals. Thesis and Dissertations.

Osborn HA. Haley AB, Hathorne CE, Flögel S, Frank M. 2014. Neodymium isotopes and concentrations in Caribbean Seawater: Tracing water mass mixing and continental input in a semi-enclosed ocean basin. Earth and Planetary Science Letters. 406. p. 174 - 186

Pahnke K, Flierdt Tvd, Jones KM, Lambelet M, Hemming SR, Goldstein SL. 2012. GEOTRACES intercalibration of neodymium isotopes and rare earth element concentrations in seawater and suspended particles. Part 2: Systematic tests and baseline profiles. Limnol. Oceanogr.: Methods. p. 252 - 269.

Pahnke K, Goldstein SL, Hemming SR. 2008. Abrupt changes in Antarctic Intermediate Water circulation over the past 25,000 years. Nature. p. 870 - 874.

Pal Singh S, Singh SK, Goswami V, Bhushan R, Rai VK. 2012. Spatial distribution of dissolved neodymium and eNd in the Bay of Bengal: Role of particulate matter and mixing of water masses. Geochimica et Cosmochimica Acta. p. 38 - 56.

Peña-Molino B, Joyce MT, Toole JM, 2011. Recent changes in the Labrador Sea Water within the Deep Western Boundary Current southeast of Cape Cod. Deep-Sea Research. 58. p. 1019 – 1030.

Perez FF, Vazquez-Rodrıguez M, Louarn E, Padın XA, Mercier H, Rıos AF. 2008. Temporal variability of the anthropogenic CO2 storage in the Irminger Sea. Biogeosciences. p. 1669 - 1679

Pickart RS, Smethie WM. 1993. How Does the Deeo Western Boundary Current Cross the Gulf Stream? : Journal of Physical Oceanography p. 2602 - 2616.

Pickart RS, Smethie WM, Lazier JRN, Jones EP. 1996. Eddies of newly formed upper Labrador Sea water. Journal of Geophysical Research p. 20711 - 20726.

Piepgras DJ, Wasserburg GJ. 1982. Composition of Neodymium in Water from the Drake Passage. Science. p. 207 - 214.

Piepgras DJ, and Wasserburg GJ, 1983. Influence of the Mediterranean outflow on the isotopic composition of neodymium in waters of the North-Atlantic. J. Geophys. Res. Oceans Atmos. 88. p. 5997 – 6006.

Piepgras DJ, and Wasserburg GJ, 1985. Strontium and neodymium isotopes in hot springs on the East Pacific Rise and Guaymas Basin. Earth and Planetary Science Letters. 72(4). p. 341 – 356.

Piepgras DJ, Wasserburg GJ. 1987. Rare earth element transport in the western North Atlantic inferred from Nd isotopic observations Geochimica et Cosmochimica Acta. p. 1257 - 1271.

Pin C, Zalduegui JFS. 1997. Sequential separation of light rare-earth elements, thorium and uranium by miniaturized extraction chromatography: Application to isotopic analyses of silicate rocks. Analytica Chimica Acta. p. 79 - 89.

Piotrowski AM, Galy A, Nicholl JAL, Roberts N, Wilson DJ, Clegg JA, Yu J. 2012. Reconstructing deglacial North and South Atlantic deep water sourcing using foraminiferal Nd isotopes. Earth and Planetary Science Letters. p. 289 - 297

Rempfer J, Stocker TF, Joos F, Dutay J-C. 2012a. Sensitivity of Nd isotopic composition in seawater to changes in Nd sources and paleoceanographic implications. Geophysical Research.

Rempfer J, Stocker TF, Joos F, Dutay J-C. 2012b. On the relationship between Nd isotopic composition and ocean overturning circulation in idealized freshwater discharge events. Paleoceanography. p. 1 - 24.

Rempfer J, Stocker TF, Joos F, Dutay J-C, Siddall M. 2011. Modelling Nd-isotopes with a coarse resolution ocean circulation model: Sensitivities to model parameters and source/sink distributions. Geochim. Cosmochim. Acta. p. 5927 - 5950.

Rickli J, Frank M, Halliday AN, 2009. The hafnium-neodymium isotopic composition of Atlantic seawater. Earth and Planetary Science Letters. 280. p. 118-127

Rutberg RL, Hemming SR, Goldstein SL. 2000. Reduced North Atlantic Deep Water flux to the glacial Southern Ocean inferred from neodymium isotope ratios Nature. p. 935 - 938.

Schlitzer R. 2013. Ocean Data View.

Schmitz JW and McCartney SM, 1993. On the North Atlantic Circulation. Review of Geophysics. 31. p. 29 – 49.

Shabani MB, Akagi T, Masuda A. 1992. Preconcentration of trace rare-earth elements in seawater by complexation with bis(2-ethylhexyl) hydrogen phosphate and 2-ethylhexyl dihydrogen phosphate adsorbed on a C18 cartridge and determination by inductively coupled plasma mass spectrometry. Anal. Chem. p. 737 - 743.

Siddall M, Khatiwala S, Flierdt Tvd, Jones K, Goldstein SL, Hemming S, Anderson RF. 2008. Towards explaining the Nd paradox using reversible scavenging in an ocean general circulation model. Earth and Planetary Science Letters. p. 448 - 461.

Smethie WM. 1993. Tracing the thermohaline circulation in the western North Atlantic using chlorofluorocarbons. Progress in Oceanography. p. 51 - 99.

Smethie WM, Fine RA, Putzka A, Jones EP. 2000. Tracing the flow of North Atlantic Deep Water using chlorofluorocarbons. Journal of Geophysical Research. p. 14297 - 14323.

Stichel T, Frank M, Rickli J, Haley BA, 2012. The hafnium and neodymium isotope composition of sweater in the Atlantic sector of the Southern Ocean. Earth and Planetary Science Letters. 317-318. p. 282-194

Stichel T, Hartman EA, Duggan B, Goldstein LS, Scher H, Pahnke K, 2014. Separating biogeochemical cycling of neodymium from water mass mixing in the Eastern North Atlantic. Earth and Planetary Science letters.

Stommel H. 1965. The Gulf Stream: A Physical and Dynamical Description University of California Press, Berkeley. p. 248.

Stramma L, Kieke D, Rhein M, Schott F,Yashayaev I, Koltermann PK, 2004. Deep water changes at the western boundary of the Subpolar North Atlantic during 1996 to 2001. Deep-Sea Research. 51. p. 1033 – 1056.

Tachikawa K, Athias V, Jeandel C. 2003. Neodymium budget in the modern ocean and paleo-oceanographic implications. Journal of Geophysical Research-Oceans.

Tanaka T, Togashi S, Kamioka H, Amakawa H, Kagami H, Hamamoto T, Yuhara M, Orihashi Y, Yoneda S, Shimizu H et al. . 2000. JNdi-1: a neodymium isotopic reference in consistency with LaJolla neodymium. Chemical Geology. p. 279 - 281.

Tanhua T, Olsson KA, Jeansson E. 2005. Formation of Denmark Strait overflow water and its hydro-chemical composition. Journal of Marine Systems. p. 264 - 288.

Toole JM, Curry RG, Joyce TM, McCartney M, Pena-Molino B. 2011. Transport of the North Atlantic Deep Western Boundary Current about 391N, 701W: 2004–2008. Deep-Sea Research II. p. 1768 - 1780.

Tsuchiya M. 1989. Circulation of the Antarctic Intermediate Waterin the North Atlantic Ocean. Journal of Marine Research. p. 747 - 755.

Van Sebille E, Baringer OM, Johns EW, Meinen SC, Beal ML, Femke de Jong M, van Aken HM, 2011. Propagation pathways of classical Labrador Sea water from its source region to 26–N, Journal of Geophysics. p. 116.

Vazquez-Rodrıguez M, Perez FF, Velo A, Rıos AF, Mercier H. 2012. Observed acidification trends in North Atlantic water masses. Biogeosciences. p. 5217 - 5230.

Weiss RF, Bullister JL, Gammon RH, Warner MJ. 1985. Atmospheric chlorofluoromethanes in the deep equatorial Atlantic. Nature. p. 608 - 610.

Worthington LV. 1959. The 18-degree water in the Sargasso Sea. Deep-Sea Research. p. 297 - 305.